

Skeletal muscle wasting and myogenic stem cells in cancer

by

Nina Esfandiari

A thesis submitted in partial fulfillment of the requirements for the degree of

Master of Science

Department of Oncology
University of Alberta

© Nina Esfandiari, 2014

Abstract

The purpose of this work is to understand properties of skeletal muscle of cancer patients experiencing severe muscle depletion. These studies were done using computed tomography (CT) imaging and patient information (demographics), and collection of muscle biopsies to analyze using flow cytometry, histology, and immunohistochemistry. In study 1, CT data was used to provide an explanatory analysis for radiation attenuation of muscles of cancer patients, a characteristic associated with muscle triglyceride content. Multivariate linear regression analysis revealed that lower muscle radiation attenuation is associated with older age, increased adipose mass, reduced muscle mass and advanced disease. In study 2, CT data and muscle biopsies were used to provide an exploratory examination of muscle morphology and cell composition. Results support the presence of muscle atrophy and a pathological infiltration of fat within muscle. These results will guide future investigations of muscle cell biology and pathology in cancer patients.

Preface

This thesis contains figures in Chapter 3 that include data from research led by Dr. V. Baracos, Dr. V. Mazurak, and Dr. C.T. Putman. All other components of this thesis are my original work.

This thesis is included in a research project that received ethics approval from the Alberta Cancer Research Ethics Board, “Molecular Profiles of Cachexia”, ETH 21709.

Chapter 2 has been published as N. Esfandiari, S. Ghosh, C.M.M. Prado, L. Martin, V. Mazurak, and V. Baracos, “Age, obesity, sarcopenia, and proximity to death explain reduced mean muscle radiation attenuation in patients with advanced cancer,” *Journal of Frailty and Aging*, 2014, vol. 3, issue 1, 3-8. My contributions as author of the article included design, data analysis, interpretation, and manuscript composition. S. Ghosh was involved data analysis, interpretation, and manuscript edits. C.M.M Prado and L. Martin were involved in data collection and manuscript edits. V. Mazurak was involved in manuscript edits. V. Baracos was the supervisory author and was involved with concept formation, interpretation, and composition of the manuscript.

Acknowledgements

I would first like to thank my supervisor, Vickie Baracos. Throughout the years, I have experienced the full extent of your wisdom, compassion, and support. I am very grateful that I was able to begin and develop a career of research under your guidance.

I would also like to thank my committee members, Vera Mazurak, Todd McMullen, and Ted Putman for the efforts they made in allowing this project to go forward and providing their different areas of expertise.

Thank you to Frank van Landeghem for assisting and providing some insight regarding skeletal muscle pathology for this project.

To my coworkers and fellow graduate students at the Cross Cancer Institute and Li Ka Shing, - thank you for the encouragement, and friendship.

Thank you to my family. I cherish the love and support with which you have surrounded me.

Lastly, I am thankful to the patients, without whom this project would not have taken place.

Table of Contents

CHAPTER 1: Introduction and literature review

1.1 Introduction.....	1
1.2 Characteristics of skeletal muscle in cancer patients.....	2
1.2.1 Quantification of skeletal muscle.....	2
1.2.2 Skeletal muscle quantification and cancer.....	3
1.2.3 Fatty Infiltration.....	4
1.3 Skeletal muscle stem cells.....	5
1.3.1 Characteristics and overview of types of stem cells in skeletal muscle.....	5
1.3.2 Stem cells in non-cancer populations.....	8
1.3.3 Stem cells in cancer populations.....	10
1.4 Summary.....	12
1.5 Hypothesis.....	13
1.6 Objectives.....	14
Figures.....	15
References.....	99

CHAPTER 2: Age, obesity, sarcopenia, and proximity to death explain reduced mean muscle radiation attenuation in patients with advanced cancer

2.1 Introduction..... 23

2.2 Methods..... 24

2.2.1 Population Cohorts..... 24

2.2.2 CT Image Analysis 99

2.2.3 Statistics..... 26

2.3 Results..... 27

2.3.1 Patient characteristics at baseline..... 27

2.3.2 Change in muscle radiation attenuation over time to death in longitudinal cohort . 28

2.4 Discussion..... 28

Tables..... 32

Figures..... 35

References..... 37

CHAPTER 3: Exploratory analyses of human muscle biopsies provide evidence of atrophy and fat infiltration in cancer-associated muscle wasting

3.1 Introduction..... 41

3.2 Methods..... 44

3.2.1 Muscle Biopsies..... 44

3.2.2 Cell isolation..... 45

3.2.3 Flow cytometry..... 46

3.2.4 Histology..... 47

3.2.5 Immunofluorescence..... 48

3.2.6 Myosin heavy chain analysis..... 49

3.2.7 Lipid analysis..... 49

3.2.8 Computed tomography image analysis..... 51

3.3 Results..... 51

3.3.1 Development of cell isolation protocol..... 51

3.3.2 Radiological characteristics of skeletal muscle of patients who consented to biopsy represent the distribution seen in larger cohorts of cancer patients..... 52

3.3.3 Morphological analyses of muscle tissue sections..... 53

3.3.4 Stem cell populations in muscle wasting: preliminary data..... 55

3.4 Discussion..... 55

Tables..... 62

Figures.....	75
References.....	86

CHAPTER 4: Final Discussion

4.1 Introduction..... 91

4.2 Human muscle biopsies are taken too infrequently and sporadically in the cancer setting to provide an absolute conclusion for skeletal muscle wasting 92

4.3 Stem cell and fatty infiltration properties not well characterized or may not necessarily translate to humans..... 94

References..... 99

List of Tables

Table 2-1

Characteristics and computed tomography image analysis at baseline for all patients, and advanced cancer patients with multiple scans only

Table 2-2

General linear model regression analysis of muscle radiation attenuation at baseline (continuous variable)

Table 2-3

General linear model regression analysis of factors associated with change in muscle radiation attenuation (continuous variable)

Table 3-1

Current literature on morphological analyses of muscle from biopsies of cancer patients.

Table 3-2

Cell isolation procedures.

Table 3-3

Antibody combinations used in flow cytometry analysis.

Table 3-4

Cell counts per milliliter of cell suspension assessed under haemocytometer.

Table 3-5

Skeletal muscle profile of male cancer patients with histological and immunofluorescent analyses.

Table 3-6

Extremes of phenotype: Direct comparison of skeletal muscle profile of male cancer patients P14 and P24.

List of Figures

Figure 1-1

Skeletal muscle stem cell map

Figure 2-1

Two lung cancer patients with low (A) and high (B) mean muscle radiation attenuation

Figure 2-2

Change in muscle radiation attenuation and tissue cross sectional area across months to death

Figure 3-1

Satellite cell and multipotent progenitor life cycles

Figure 3-2

Pathological classification of intermuscular adipose tissue and intramyocellular lipid droplets.

Figure 3-3

Muscle biopsy patients placed within larger cohort of lung and gastrointestinal cancer patients (n=828) for muscle cross-sectional area (A) and attenuation (B).

Figure 3-4

Z-scores of muscle cross-sectional area and attenuation for muscle biopsy patients within larger dataset of patients.

Figure 3-5

Computed tomography images analyzed for patients P14 (A) and P24 (B).

Figure 3-6

Haematoxylin and eosin staining of tissue sections from patients P14 and P24 allow measurements of myofibres and exhibit abnormalities in wasting.

Figure 3-7

Haematoxylin and eosin and Oil Red O staining of tissue sections from patients P14 and P24 highlight areas of fat in and between muscle.

Figure 3-8

Multipotent, adipogenic, and myogenic progenitors identified in interstitium of skeletal muscle.

Figure A1

Infiltration of myofibres with CD68+ inflammatory cells.

List of Abbreviations

APC, allophycocyanin

CSA, cross-sectional area

CD, cluster of differentiation

CT, computed tomography

FAPs, fibroadipogenic precursors

FBS, fetal bovine serum

FC, flow cytometry

FITC, fluorescein isothiocyanate

GC-FID, gas chromatography with flame ionization detector

H&E, Haematoxylin and Eosin

IF, immunofluorescence

IMAT, intermuscular adipose tissue

L3, third lumbar vertebrae

MA, muscle radiation attenuation

MHC, myosin heavy chain

MCSA, myofibre cross-sectional area

MNC, mononuclear cell

ORO, Oil red O

PAX, paired box transcription factor

PE, phycoerythrin

PICs, PW1+/Pax7- interstitial cells

PBS, phosphate buffered saline

PW1, paternally expressed gene 3, also known as Peg3

RA, rectus abdominis

RBC, red blood cell

SAT, subcutaneous adipose tissue

SC, satellite cell

SMI, skeletal muscle index

TAT, total adipose tissue

VAT, visceral adipose tissue

Units of Measure:

cm², centimeter(s) squared

m², meter(s) squared

g, gram

kg, kilogram

HU, Hounsfield Units

kVp, peak kilovoltage

mA, milliamperere

μg, microgram

μm, micrometer

μL, microliter

CHAPTER 1: Introduction and literature review

1.1 Introduction

Skeletal muscle is a plastic organ. It adapts to a variety of physiological signals, messengers that signal storage and mobilization of energy, performance of activity, and regeneration following injury. With aging, both muscle mass and regenerative capacity are progressively lost (1, 2). Severe skeletal muscle depletion is known as sarcopenia, often arising in elderly as well as in cancer patients. Sarcopenia is associated with multiple factors such as decreased physical activity and food intake, increased inflammation and pathological infiltration of muscle with fat (3).

Sarcopenia is one of the most prominent aspects of cachexia. Cachexia is a multi-factorial and multi-organ syndrome that is characterized by a loss of skeletal muscle mass with or without loss of fat mass (4). The primary criterion for cachexia is involuntary weight loss; however much of the work to understand cachexia has investigated loss of skeletal muscle mass. Cachexia is associated with chronic inflammatory diseases such as cancer and accounts for up to 20-30% of cancer patient deaths (5). It is also associated with a decreased quality of life, as well as increased morbidity and mortality. Cachexia occurs due to a combination of reduced food intake and abnormal metabolism.

Breakdown of energy stores within muscle is partly mediated through pro-inflammatory cytokines. In cancer cachexia, there is added interplay between host metabolism, pro-inflammatory cytokines, and the energetically demanding tumor, which serves to perpetuate an inflammatory, dysmetabolic state.

Assessment of skeletal muscle can be completed at several levels – cellular, tissue, and whole-body. It has been proposed that sarcopenia is due to an imbalance in the

population of stem cells found within skeletal muscle (6, 7), though this has not been directly examined in humans. In cancer patients especially, whole-body volumes of muscle have been investigated, but cellular and structural components of skeletal muscle in cancer have been rarely explored. Recent interest has surrounded activity of myogenic stem cells in several myopathies (i.e. diseases of muscle) (8-11). With a better understanding of contributors to muscle repair and regeneration, stem cells have the potential to be manipulated to be involved in therapies for muscle wasting as well.

1.2 Characteristics of skeletal muscle in cancer patients

1.2.1 Quantification of skeletal muscle

Assessment of skeletal muscle has developed over the past few decades as a significant component of the cancer trajectory. Measurements of cancer patients include body weight and height to provide the body mass index (BMI) of an individual. However, the internal composition of each person with similar BMIs can differ greatly (12, 13). Body composition analysis distinguishes fat from fat-free tissues, providing more detail about the body. Several methods have been used in the past such as dual energy x-ray scans, magnetic resonance imaging, and computed tomography (CT) images (14). The analysis of CT images are now considered the gold standard in determining body composition due to its precision and its specificity in distinguishing muscle from other tissues (15). Though CT imaging exposes individuals to high radiation doses, this is not an issue with cancer patients, who have CT images routinely taken throughout their cancer trajectory to determine tumor characteristics.

Analysis of CT images involves the identification of suitable vertebral landmarks, such as the third lumbar vertebrae (L3), in a series of axial images. At this level, specific

ranges of radiation attenuation are used to evaluate each tissue. Attenuation is the radiodensity of a tissue that is dependent upon how easily it is penetrated by energy. Attenuation is measured in Hounsfield Units (HU), a linear scale based on water (0 HU) and air (-1000 HU). The cross-sectional area (CSA, cm^2) of skeletal muscle, as well as visceral, subcutaneous, and intermuscular adipose tissue can be measured by the product of the number of pixels with attenuation values appropriate to their corresponding tissues and the area represented per pixel in the image. From values determined for muscle, the skeletal muscle index (SMI) can be determined as the CSA normalized to the square of height (m^2) of the individuals or can be used to estimate the whole body volumes of tissue. Estimation of whole body volumes of muscle or adipose tissue has been done in healthy adults (16), cirrhotic patients (17, 18), and cancer patients (19). SMI enables determination of whether an individual is sarcopenic, which places them at greater health risk than a non-sarcopenic individual. The mean muscle radiation attenuation (MA) may also indicate fat infiltration, though this has not yet been standardized (20). Reduced MA has been demonstrated in cancer patients and corresponds to pathological fat infiltration (myosteatorsis), which has been associated with poor survival in cancer patients (13, 21, 22).

1.2.2 Skeletal muscle quantification and cancer

Evaluation of skeletal muscle in cancer has gained some popularity as it significantly correlates to several clinical outcomes. Muscle loss is associated with loss of strength and function, greater risks of falls and fractures, longer hospital stays (23), chemotherapy toxicity (24, 25), poor response to surgery (26), and decreased overall survival (12, 21, 22, 27). Therefore, skeletal muscle depletion is a significant prognostic

indicator in cancer (13, 22 27-29) as well as in other patient populations such as cirrhosis patients (17). A study of 1473 cancer patients illustrated that sarcopenia is predictive of a poor prognosis regardless of BMI (13).

Investigations of muscle depletion have been documented using CT imaging. Skeletal muscle has been shown to be lost in the clinical setting (30), and can be concurrent with fat loss. In one cohort of 368 advanced cancer patients who had at least two CT scans over their disease trajectory, muscle loss was observed in 40% of the intervals between two scans (30). Being within three months from death was a particularly significant risk factor for loss of muscle. However, a percentage of patients exhibited the ability to gain muscle, particularly when they were showing disease response to therapy. The characterization of the cell biology and muscle structure of patients who either lose or gain muscle mass would provide information to differentiate the behaviours of stem cells comprising muscle tissue, which presumably underlie hypertrophy and atrophy.

1.2.3 Fatty infiltration

Though sarcopenia has been defined as reduced quantity of skeletal muscle, another characteristic is a decreased quality and strength of muscle due to infiltration of fat (31, 32). Fat infiltration can be either intramyocellular (within muscle fibres) or adipocytes in the perimysium. Both of these can be physiological, as fat is stored in muscle to fuel aerobic activity. However, in large quantities, and in those who are losing muscle, fat deposition can also be pathological (33). Increased intramuscular lipids (34) and intermuscular adipocytes (35) can be observed in older individuals (36), and have been associated with insulin resistance, obesity, and type II diabetes (35).

Fatty infiltration can be estimated by evaluating intermuscular adipose tissue and average MA values measured through CT image analysis. As the attenuation ranges of fat are lower than those of muscle, reduced mean MA indicates greater infiltration of the muscle with fat. However, due to the non-standard criteria for measuring mean muscle radiation attenuation, it is difficult to compare results between studies (20). Fat infiltration measured by mean MA has been revealed as a prognostic indicator of survival in various forms of cancer (13, 21, 22).

1.3 Skeletal muscle stem cells

1.3.1 Characteristics and overview of types of stem cells in skeletal muscle

Much of the work performed on skeletal muscle stem cells has been on animal models and cell lines. Due to the difficulty in acquiring muscle biopsies, not as much is known about stem cell populations in humans, particularly cancer patients. The significance of sarcopenia within the clinical setting requires a greater understanding of its pathophysiology. Regeneration of skeletal muscle, particularly at a cellular level, needs to be explored to determine specific deviations in mechanisms that may occur in individuals with sarcopenia compared to those without sarcopenia. Roles and interactions of stem cells found within skeletal muscle reveal a very complex picture (**Figure 1-1**). Some stem cells follow a strict lineage, such as the satellite cells (SCs), and some may follow multiple lineages depending upon the signals they receive from their environment. Non-satellite stem cells that follow the myogenic lineage can be found in the interstitium, or the area between muscle fibres. These include mesoangioblasts, pericytes, multipotent progenitors, PW1+/Pax7- interstitial cells (PICs), and the side population. There are also stem cells that can become adipogenic, such as the multipotent

progenitors (10) and fibroadipogenic progenitors (FAPs). FAPs can also form fibrotic tissue (37).

Animal models have been used to isolate a specific stem cell population of interest, though no model has been created to determine how all the populations work together. Also, due to the fact that some populations (PICs, FAPs) have only recently been discovered in mouse tissue (37, 38), it is not known whether they exist in humans. These differences are further intensified because certain nuclear and cell surface antigens identified in humans may not be present in rodents, and vice versa. However, it is generally accepted that satellite cells are the primary contributors to skeletal muscle regeneration and repair. Other stem cells may also participate in muscle regeneration, and are believed to aid in facilitating these processes as efficiently as possible (39). As nuclei within myofibres of skeletal muscle are mitotically arrested, they are unable to replicate and respond to growth or injury. Satellite cells, named due to the peripheral position of the cell between the basal lamina and sarcolemma of the myofibre (40), are normally quiescent in adult muscle, comprising ~2-4% of total nuclei found within skeletal muscle. In response to muscle damage or growth stimulus, SCs are activated, exiting the cell cycle and undergoing rounds of proliferation before differentiating into myocytes that may fuse to each other or pre-existing myofibres. SCs may be identified at each of their stages through a variety of nuclear and cell surface antigens referred to as myogenic regulatory factors. Quiescent SCs express the transcription factors Pax3 and Pax7, and cell surface marker CD56 (neural cell adhesion molecule). When committed, SCs lose expression of the early stage marker Pax3. At this point, SCs may return to their quiescent state, sustaining the pool of SCs available for regeneration (7) or become

activated to be proliferating myoblasts, with an upregulation of the muscle-specific transcription factor, MyoD. These myoblasts may differentiate into myocytes with the expression of another muscle-specific marker, myogenin, and concomitant loss of Pax7 and CD56 expression. Myocytes may then fuse with each other or existing myocytes to contribute to muscle growth and repair.

Other stem cells may also participate in muscle regeneration, though it is not completely understood the extent of their involvement or how these cells interact with SCs in humans. PICs are named due to their location in the interstitium between myofibres and are distinct from SCs in that they do not express Pax7 (38). PICs express PW1, an early marker of myogenic lineage, and contribute to muscle growth and repair with the aid of SCs. They are bipotent, so they may contribute to either smooth or skeletal myogenesis. They are able to proliferate to become either PICs or SCs (38). The side population can also contribute to either myogenesis or to the satellite cell pool (41). The existence of these two populations indicates that there may be a capacity to replace SCs in the event that the SC population is depleted, though this may to a very limited extent.

Some non-satellite stem cells can also follow multiple lineages. Recent works have highlighted a role for pericytes in fibrosis due to chronic injury (42), however the main role of pericytes isolated from skeletal muscle has been the ability to participate in skeletal or smooth myogenesis (43, 44). Multipotent progenitors are a recently discovered group of stem cells observed to follow multiple lineages in humans (10). These cells are positive for CD56, as well as CD34 and CD15. However, they may lose expression of either CD15 to become myogenic or lose the expression of CD56 to become adipogenic in nature (10, 45).

FAPs are developmentally distinct from SCs and other myogenic progenitors, in that they do not have myogenic potential (37). They are found in abundance in the muscle interstitium but can also be found adjacent to injured in myofibres damaged muscle, indicating that they play an indirect role in myogenesis. They have two roles when responding to damage, depending upon signals they receive from the environment. FAPs can contribute to the degeneration of the muscle by differentiating into adipose or connective tissue (46), or when co-cultivated with myogenic progenitors, they may also promote regeneration by releasing pro-differentiation signals (37, 47).

Overall, there is some evidence in animal models to provide an insight into the functions and relationships between these stem cells. Despite involvement of other cells, it is still believed that satellite cells participate most significantly in muscle regeneration and repair, and that other cells are involved in the fine-tuning of the myogenic process. For example, pericytes require co-culture with pre-existing myoblasts to differentiate into myocytes (44). The varieties of cell types also highlight the significance of stem cells in maintaining a balance between a myogenic and non-myogenic stem cell fate.

1.3.2 Stem cells in non-cancer populations

Additional contributors to sarcopenia could be shifts in the proportion and activities of different cell populations found in skeletal muscle, including SCs. Though some mouse studies have been done (9, 48) in terms of muscle wasting, the changes to the mechanisms behind muscle stem cells in humans are not well understood, thus the role of SCs in the pathogenesis of sarcopenia are still under debate. It is believed that muscle wasting in the older population could be due to the inability for muscle to repair itself after bouts of activity, which eventually could contribute to sarcopenia. There is

also still no agreement about whether it is changes to the stem cell niche or weakening of the stem cells due to age that prevent the stem cells from responding to environmental cues to their full capacity (or both) (49). Similarly, an underlying factor contributing to sarcopenia may be a change in SC number or activity at any stage. Experimental studies in rodent models indicate that there is no loss in SC number, and that it is the function of the SC that is impacted by age (50). However, it remains equivocal if the same applies in humans (51), or if loss of both SC number and activity (52) could contribute to the loss of regenerative potential.

Most of the work done to date on SCs in humans has compared younger and older subjects and effects of exercise. Several studies have found that older subjects (~70 years of age) have 35-50% of the number of SCs as the younger populations (~21 years of age) (53, 54). After bouts of activity, the number of SCs in the younger population nearly doubled after 48 hours, whereas this increase was not observed in the older population (53). These observations imply that there is a need for SCs during regeneration and further reinforces the idea that a fewer number of SCs may explain the decreased ability to regenerate muscle in older subjects. This may contribute to the lack of maintenance and repair of tissue in older muscle over time. Also, whereas in aged mice muscle it seems that SCs have lost the ability to complete their myogenic program, aged human muscle has fewer SCs to begin with that cannot differentiate into myotubes. Similarly, in comparison to healthy tissue, patients with muscular dystrophy had significantly fewer myogenic and significantly more adipogenic cells in their muscle tissue. The behavior of this cell population supports the idea that certain stem cells in tissue from individuals with myopathies may be rerouted to follow a non-myogenic lineage (10).

Recent advances have also been made in the area of muscular dystrophy in regards to treatments involving mesoangioblasts. Mesoangioblasts were found to have regenerative properties in animal models of muscular dystrophy (55) and are consequently part of a clinical trial currently being conducted (56). These cells show the therapeutic potential for stem cells in myopathies. Though other non-satellite stem cells (such as PICs and FAPs) have not been investigated in humans with age-related muscle loss, their myogenic roles implicate that they are cells of interest and may call for further study.

1.3.3 Stem cells in cancer populations

The current literature on SCs, and more generally stem cells, in cancer patients is very limited. One recent article has attempted an investigation into the involvement of SCs in cancer cachexia (8), by quantifying the number of SCs as cells positive for Pax7 between the basal lamina and sarcolemma. There were 60% more Pax7+ cells in tissue from cachectic patients than control subjects, indicating an expansion of SCs, particularly in cancer patients with greater weight loss. In the same study, a concurrent investigation of mouse skeletal muscle led to the conclusion that it is the overexpression of Pax7 that leads to the wasting of muscle, as it inhibits the differentiation phase of the myogenic program, a finding shared in a previous study done on cultured cells (57). However, these results could also be due to the actions of other cells or signals affecting satellite cells and preventing them from committing to myogenesis, and the buildup of Pax7 is merely the replication of Pax7+ cells attempting to repair the damaged muscle.

Several limitations can also be noted in this study. He et al. stratified patients based on weight loss rather than muscle loss. Staining for IgG, a marker for damage and

electron microscopy images were performed to illustrate muscle damage. However, the magnification in electron microscopy is too high to accurately represent the entire muscle, and despite both of these assessments, muscle damage does not indicate loss of muscle mass in the patients. Also, ages of patients and healthy subjects from whom muscle biopsies were taken ranged from 27 to 82 years of age (with the cancer group including older individuals). Since age affects SC number, these results may not have been due to cancer cachexia, per se. Lastly, Pax7 is a marker that is observed in multiple types of SCs (i.e. quiescent and committed SCs, proliferating myoblasts). In this study, all Pax7-positive SCs were measured and thus the individual proportions of these subpopulations are not known. Additional information about these populations may have been provided with the use of additional antibodies for the SC markers. This may also provide some insight as to whether the presence of other cell types prevents the cells from entering the differentiation phase of the life cycle or whether Pax7 acts alone. As this is the first and only published article on SCs in cancer cachexia, there is room for further investigation on the fate of these cells.

1.4 Summary

Cancer patients experience significant skeletal muscle loss. It is important to understand mechanisms that may be driving this at a cellular level. There is evidence that specific stem cell populations are altered during aging or myopathies, either by decreasing in number or altering their normal myogenic program. Persistent changes to cells may result in depletion of muscle over time. Other characteristics of skeletal muscle, such as morphology and the infiltration of fat and immune cells, may also contribute to this phenomenon. By mapping changes that occur in the life of a stem cell and characterizing human muscle, a greater understanding of the wasting process can be attained. In particular, interactions between specific stem cells, or between the cells and the environment, may play a key role in this wasting. With further investigations in human subjects, future studies may explore the realm of therapies involving altered stem cell behaviour.

1.5 Hypothesis

The purpose of this thesis is to investigate the following hypotheses:

- 1) Cancer patients with the greatest muscle wasting will have a lower number of stem cells that will follow a myogenic lineage and a higher number of stem cells that will follow an adipogenic lineage.
- 2) Skeletal muscle from cancer patients with the greatest wasting will exhibit structural abnormalities associated with atrophy.
- 3) Cancer patients with low muscle radiation attenuation will have higher total adipose tissue, lower skeletal muscle mass, and poorer survival than those with higher muscle radiation attenuation.

1.6 Objectives

The objectives of this thesis are the following:

Investigated in Chapter 2:

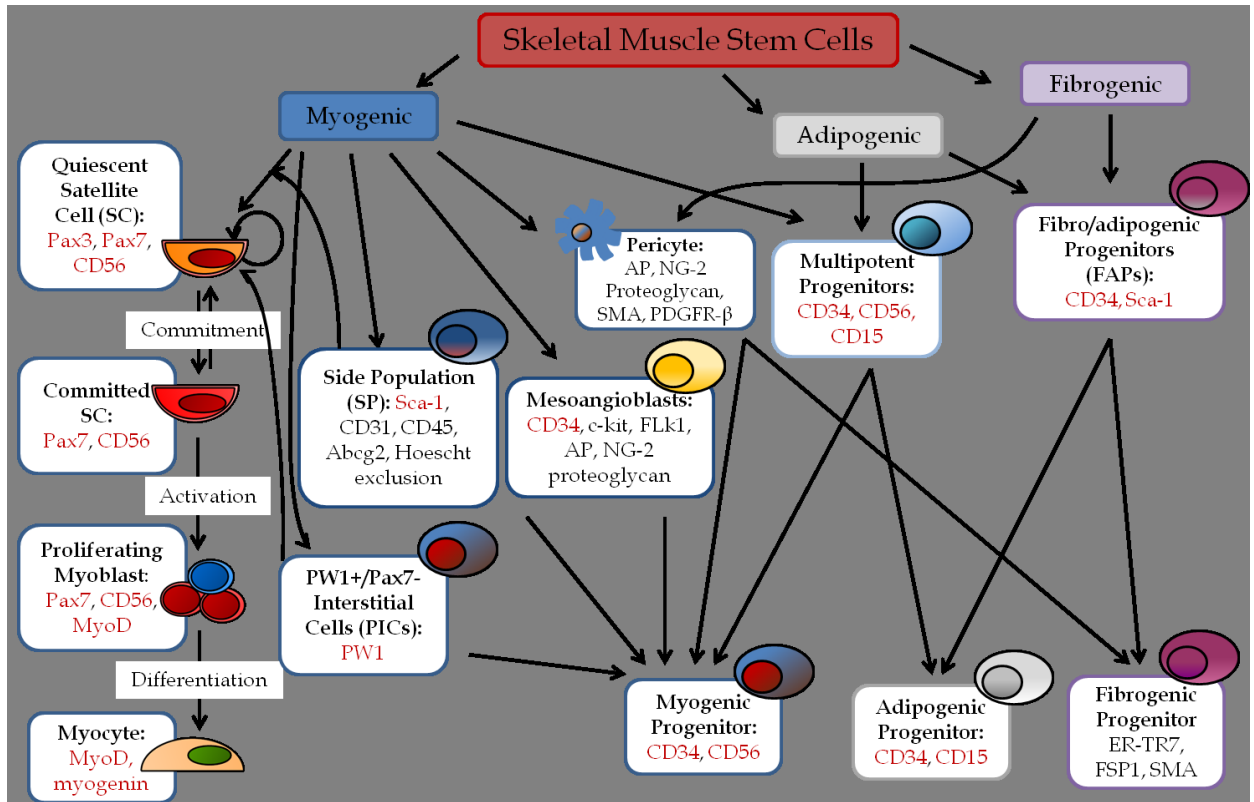
- 1) To create an explanatory model of muscle radiation attenuation in a large cohort of cancer patients using multivariate statistics
- 2) To assess muscle radiation attenuation at baseline in a large and diverse cohort of cancer patients
- 3) To evaluate changes in muscle radiation attenuation over time in relation to disease progression

Investigated in Chapter 3:

- 1) To develop a method for the isolation of mononuclear cells from muscle biopsies to enable preservation of adipocytes
- 2) To determine the proportion of stem cells dedicated to the myogenic or adipogenic program
- 3) To determine whether there are higher adipogenic ($CD34^+CD15^+$) stem cells in wasting muscle than healthy muscle

Figures

Figure 1-1: Skeletal muscle stem cell map



Skeletal muscle stem cells that may follow a myogenic, adipogenic, or fibrogenic lineage.

These include satellite cells, the main contributors to myogenesis and muscle repair, as well as PW1+/Pax7- interstitial cells, mesoangioblasts, pericytes, multipotent progenitors, fibroadipogenic progenitors, and the side population. SC: satellite cells, FAPs: fibroadipogenic progenitors, PICs: PW1+/Pax7- interstitial cells, SP: side population, CD: cluster of differentiation, PAX: paired box protein.

References

1. Baumgartner RN, Koehler KM, Gallagher D, et al. Epidemiology of sarcopenia among the elderly in New Mexico. *Am J Epidemiol.* 1998;147(8):755–763.
2. Carlson ME, Conboy IM. Loss of stem cell regenerative capacity within aged niches. *Aging Cell.* 2007;6(3):371–382.
3. Johns N, Stephens N, Fearon K. Muscle wasting in cancer. *Int J Biochem Cell B.* 2013;45(10):2215–2229.
4. Fearon K, Strasser F, Anker SD, et al. Definition and classification of cancer cachexia: an international consensus. *Lancet Oncol.* 2011;12(5):489–495.
5. Fearon K. Cancer cachexia: developing multimodal therapy for a multidimensional problem. *Eur J Cancer.* 2008;44(8):1124–1132.
6. Thornell LE. Sarcopenic obesity: satellite cells in the aging muscle. *Curr Opin Clin Nutr.* 2011;14(1):22.
7. Jang Y, Sinha M, Cerletti M, et al. Skeletal muscle stem cells: effects of aging and metabolism on muscle regenerative function. In: *Cold Spring Harbor Symposia on Quantitative Biology.* Vol 76; 2011:101–111.
8. He WA, Berardi E, Cardillo VM, et al. NF-kappaB-mediated Pax7 dysregulation in the muscle microenvironment promotes cancer cachexia. *J Clin Invest.* 2013;123(11):4821.
9. Schwarzkopf M, Coletti D, Sassoon D, et al. Muscle cachexia is regulated by a p53-PW1/Peg3-dependent pathway. *Gene Dev.* 2006;20(24):3440–3452.
10. Pisani DF, Clement N, Loubat A, et al. Hierarchization of myogenic and adipogenic progenitors within human skeletal muscle. *Stem Cells.* 2010;28(12):2182–2194.

11. Pallafacchina G, Blaauw B, Schiaffino S. Role of satellite cells in muscle growth and maintenance of muscle mass. *Nutr Metab Cardiovas*. 2012;23(S1):S12-18.
12. Prado CM, Lieffers JR, McCargar LJ, et al. Prevalence and clinical implications of sarcopenic obesity in patients with solid tumours of the respiratory and gastrointestinal tracts: a population-based study. *Lancet Oncology*. 2008;9(7):629–635.
13. Martin L, Birdsell L, MacDonald N, et al. Cancer Cachexia in the Age of Obesity: Skeletal Muscle Depletion Is a Powerful Prognostic Factor, Independent of Body Mass Index. *J Clin Oncol*. 2013;31(12):1539–1547.
14. MacDonald AJ, Greig CA, Baracos V. The advantages and limitations of cross-sectional body composition analysis. *Curr Opin Supportive Palliative Care*. 2011;5(4):342–349.
15. Mitsiopoulos N, Baumgartner R, Heymsfield S, et al. Cadaver validation of skeletal muscle measurement by magnetic resonance imaging and computerized tomography. *J Appl Physiol*. 1998;85(1):115–122.
16. Shen W, Punyanitya M, Wang Z, et al. Total body skeletal muscle and adipose tissue volumes: estimation from a single abdominal cross-sectional image. *J Appl Physiol*. 2004;97(6):2333–2338.
17. Tandon P, Ney M, Irwin I, et al. Severe muscle depletion in patients on the liver transplant wait list: Its prevalence and independent prognostic value. *Liver Transplant*. 2012;18(10):1209–1216.
18. Montano-Loza AJ, Meza-Junco J, Baracos VE, et al. Severe muscle depletion predicts postoperative length of stay but is not associated with survival after liver transplantation. *Liver Transplant*. 2014;20(6):640-648.

19. Mourtzakis M, Prado CM, Lieffers JR, et al. A practical and precise approach to quantification of body composition in cancer patients using computed tomography images acquired during routine care. *Appl Physiol Nutr Metabol*. 2008;33(5):997–1006.
20. Aubrey J, Esfandiari N, Baracos V, et al. Measurement of skeletal muscle radiation attenuation and basis of its biological variation. *Acta Physiol*. 2014;210(3):489-497.
21. Antoun S, Lanoy E, Iacovelli R, et al. Skeletal muscle density predicts prognosis in patients with metastatic renal cell carcinoma treated with targeted therapies. *Cancer*. 2013;119(18):3377-3384.
22. Sabel MS, Lee J, Englesbe MJ, Holcombe S. Sarcopenia as a prognostic factor among patients with stage III melanoma. *Ann Surg Oncol*. 2011;18(13):3579–3585.
23. Cosquéric G, Sebag A, Ducolombier C, et al. Sarcopenia is predictive of nosocomial infection in care of the elderly. *Briy J Nutr*. 2006;96(5):895–901.
24. Antoun S, Baracos V, Birdsell L, et al. Low body mass index and sarcopenia associated with dose-limiting toxicity of sorafenib in patients with renal cell carcinoma. *Ann Oncol*. 2010;21(8):1594–1598.
25. Prado CM, Baracos VE, McCargar LJ, et al. Body composition as an independent determinant of 5-fluorouracil-based chemotherapy toxicity. *Clin Cancer Res*. 2007;13(11):3264–3268.
26. Bachmann J, Heiligensetzer M, Krakowski-Roosen H, et al. Cachexia worsens prognosis in patients with resectable pancreatic cancer. *J Gastr Surg*. 2008;12(7):1193–1201.
27. Meza-Junco J, Montano-Loza AJ, Baracos VE, et al. Sarcopenia as a Prognostic

Index of Nutritional Status in Concurrent Cirrhosis and Hepatocellular Carcinoma. *J Clin Gastroenterol.* 2013;47(10):861-870.

28. Lanic H, Kraut-Tauzia J, Modzelewski R, et al. Sarcopenia is an Independent Prognostic Factor in Elderly Patients with Diffuse Large B-Cell Lymphoma Treated with Immunochemotherapy. *Leuk Lymphoma.* 2014;55(4):817-823.

29. Tan BH, Birdsell LA, Martin L, et al. Sarcopenia in an overweight or obese patient is an adverse prognostic factor in pancreatic cancer. *Clin Cancer Res.* 2009;15(22):6973–6979.

30. Prado CM, Sawyer MB, Ghosh S, et al. Central tenet of cancer cachexia therapy: do patients with advanced cancer have exploitable anabolic potential? *Am J Clin Nutr.* 2013;98(4):1012–1019.

31. Goodpaster BH, Carlson CL, Visser M, et al. Attenuation of skeletal muscle and strength in the elderly: The Health ABC Study. *J Appl Physiol.* 2001;90(6):2157–2165.

32. Visser M, Kritchevsky SB, Goodpaster BH, et al. Leg muscle mass and composition in relation to lower extremity performance in men and women aged 70 to 79: the health, aging and body composition study. *J Am Geriatr Soc.* 2002;50(5):897–904.

33. Miljkovic I, Zmuda JM. Epidemiology of myosteatorsis. *Curr Opin Clin Nutr Metab Care.* 2010;13(3):260.

34. Goodpaster BH, Kelley DE, Thaete FL, et al. Skeletal muscle attenuation determined by computed tomography is associated with skeletal muscle lipid content. *J Appl Physiol.* 2000;89(1):104–110.

35. Goodpaster BH, Krishnaswami S, Resnick H, et al. Association between regional adipose tissue distribution and both type 2 diabetes and impaired glucose tolerance in elderly men and women. *Diabetes Care*. 2003;26(2):372–379.
36. Goodpaster BH, Carlson CL, Visser M, et al. Attenuation of skeletal muscle and strength in the elderly: The Health ABC Study. *J Appl Physiol*. 2001;90(6):2157–2165.
37. Joe AWB, Yi L, Natarajan A, et al. Muscle injury activates resident fibro/adipogenic progenitors that facilitate myogenesis. *Nat Cell Biol*. 2010;12(2):153–163.
38. Mitchell KJ, Pannérec A, Cadot B, et al. Identification and characterization of a non-satellite cell muscle resident progenitor during postnatal development. *Nat Cell Biol*. 2010;12(3):257–266.
39. Pannérec A, Marazzi G, Sassoon D. Stem cells in the hood: the skeletal muscle niche. *Trends Mol Med*. 2012;18(10):599-606.
40. Mauro A. Satellite cell of skeletal muscle fibres. *J Biophys Biochem Cy*. 1961;9(2):493–495.
41. Doyle MJ, Zhou S, Tanaka KK, et al. Abcg2 labels multiple cell types in skeletal muscle and participates in muscle regeneration. *J Cell Biol*. 2011;195(1):147–163.
42. Birbrair A, Zhang T, Wang Z-M, et al. Role of pericytes in skeletal muscle regeneration and fat accumulation. *Stem Cells Dev*. 2013;22(16):2298–2314.
43. Cappellari O, Cossu G. Pericytes in Development and Pathology of Skeletal Muscle. *Circ Res*. 2013;113(3):341–347.
44. Dellavalle A, Sampaolesi M, Tonlorenzi R, et al. Pericytes of human skeletal muscle are myogenic precursors distinct from satellite cells. *Nat Cell Biol*. 2007;9(3):255–267.

45. Lecourt S, Marolleau J-P, Fromigué O, et al. Characterization of distinct mesenchymal-like cell populations from human skeletal muscle *in situ* and *in vitro* *Exp Cell Res.* 2010;316(15):2513–2526.
46. Uezumi A, Fukada S, Yamamoto N, et al. Mesenchymal progenitors distinct from satellite cells contribute to ectopic fat cell formation in skeletal muscle. *Nat Cell Biol.* 2010;12(2):143–152.
47. Mozzetta C, Consalvi S, Saccone V, et al. Fibroadipogenic progenitors mediate the ability of HDAC inhibitors to promote regeneration in dystrophic muscles of young, but not old Mdx mice. *EMBO Mol Med.* 2013;5(4):626–639.
48. Reed SA, Sandesara PB, Senf SM, et al. Inhibition of FoxO transcriptional activity prevents muscle fibre atrophy during cachexia and induces hypertrophy. *FASEB J.* 2012;26(3):987–1000.
49. Fulle S, Di Donna S, Puglielli C, et al. Age-dependent imbalance of the antioxidative system in human satellite cells. *Exp Gerontol.* 2005;40(3):189–197.
50. Collins CA, Olsen I, Zammit PS, et al. Stem cell function, self-renewal, and behavioral heterogeneity of cells from the adult muscle satellite cell niche. *Cell.* 2005;122(2):289–301.
51. Pietrangelo T, Puglielli C, Mancinelli R, et al. Molecular basis of the myogenic profile of aged human skeletal muscle satellite cells during differentiation. *Exp Gerontol.* 2009;44(8):523–531.
52. McKay BR, Ogborn DI, Bellamy LM, et al. Myostatin is associated with age-related human muscle stem cell dysfunction. *FASEB J.* 2012;26(6):2509–2521.

53. McKay BR, Toth KG, Tarnopolsky MA, et al. Satellite cell number and cell cycle kinetics in response to acute myotrauma in humans: immunohistochemistry versus flow cytometry. *J Physiol*. 2010;588(17):3307–3320.
54. Carlson ME, Suetta C, Conboy MJ, et al. Molecular aging and rejuvenation of human muscle stem cells. *EMBO Mol Med*. 2009;1(8-9):381–391.
55. Sampaolesi M, Blot S, D’antona G, et al. Mesoangioblast stem cells ameliorate muscle function in dystrophic dogs. *Nat*. 2006;444(7119):574–579.
56. Fondazione Centro s, Raffaele del Monte Tabor. Cell Therapy Of Duchenne Muscular Dystrophy by intra-arterial delivery of HLA-identical allogeneic mesoangioblasts. In: Clinicaltrialsregister.eu [Internet]. Italy: Italian Medicines Agency. 2011- [cited 2014]. Available from: <https://www.clinicaltrialsregister.eu/ctr-search/trial/2011-000176-33/IT>
EudraCT Number: 2011-000176-33
57. Olguin HC, Olwin BB. Pax-7 up-regulation inhibits myogenesis and cell cycle progression in satellite cells: a potential mechanism for self-renewal. *Dev Biol*. 2004;275(2):375–388.

CHAPTER 2: Age, obesity, sarcopenia, and proximity to death explain reduced mean muscle radiation attenuation in patients with advanced cancer

2.1 Introduction

Skeletal muscle wasting is a significant component of cancer cachexia. Previous investigations have shown that reduced quantity of skeletal muscle is associated with shorter overall survival in patients with colorectal (1) and pancreatic (2) cancers, as well as cohorts of multiple cancer types (3, 4). Cross-sectional imaging with computed tomography (CT) has been used to document muscle loss during disease progression and the rate of muscle loss increases exponentially as patients approached death.

Muscle radiation attenuation (MA, often also called muscle density) is another radiologic characteristic of muscle related to a variety of outcomes. Attenuation is measured in Hounsfield Units (HU), a linear scale centered on water (0 HU). Considering the entire organ, any given skeletal muscle displays attenuation values between -190 to +150 HU, with a prominent peak around +50 HU (muscle). When muscle cross-sectional area and attenuation are reported in the literature, the most common practice is to use predefined HU ranges (5). Inter-muscular adipose tissue (fat between muscle fibres) is most commonly demarcated between -190 and -30 HU (6). The HU range used for muscle starts at either 0 HU or -29 HU and extends to 100, 150 or 200 HU. Reduced MA (i.e. as reduced mean attenuation within the preset range) is believed to reflect the pathological infiltration of muscle with fat. Fat may be found within muscle in a physiological setting as a source of energy, however reduced MA is believed to be pathological, as it has been shown to correspond closely to muscle lipid content and loss of muscle function (6). Several recent studies reported that reduced MA in cancer patients associates with poor survival in multivariate statistical models that include age, sex,

performance status, and disease characteristics (3, 7, 8). To date this has been observed in stage III melanoma (7), advanced lung and gastrointestinal tract cancers (3) and metastatic renal cell carcinoma (8). It was further suggested that MA could be incorporated into the prognostic scores for management of patients with cancer (8), though the basis for the association between MA and survival remains unknown.

The broader literature in non-malignant disease includes additional factors thought to influence MA. A decrease in MA has been illustrated in association with age (9), obesity (6), detraining (10) or degenerative conditions of the joints or spinal column (11-13) and diabetes (6). Conversely, strength and endurance training are associated with increases in MA (10, 14, 15). Our objective was to build explanatory models of MA in well-powered cohort using multivariate statistics controlling for age, sex, disease characteristics, and body composition. MA was measured at baseline from CT images taken from a large cohort of patients with various cancer diagnoses. The change in MA was also examined in relation to disease progression over time to death.

2.2 Methods

2.2.1 Population Cohorts

Details regarding the original prospective study cohorts can be found in previous publications (3, 4). Both cohorts included gastrointestinal and lung cancer patients. All studies were approved by the Alberta Cancer Research Ethics Board. Data were collected on adult patients referred to outpatient medical oncology clinics at the Cross Cancer Institute (the only tertiary cancer treatment centre serving northern Alberta, Canada; population: 1.8 million). Age, sex, dates of birth and death, cancer diagnosis, stage, and morphology were obtained from the Alberta Cancer Registry. Cancer staging was based

upon the guidelines of American Joint Committee on Cancer (version 1.04.00) groupings of stage I-IV. Included patients had cholangiocarcinoma or solid tumors of the pancreas, gastrointestinal or respiratory tracts. Patient data were collected at the time of their initial visit before treatment. Body mass index (BMI, kg/m^2) categories used were: <20.0 , underweight; $20.0-24.0$, normal weight; $25.0-29.9$, overweight; and ≥ 30.0 , obese. Baseline patient characteristics from each cohort were not significantly different for any feature. Identical results were obtained in the general linear model regression analysis of baseline MA. Thus, it was deemed justifiable to study baseline characteristics after merging the two data sets at initial assessment.

2.2.2 CT Image Analysis

CT images were completed with a spiral CT scanner for initial staging and routine diagnostic purposes. Patients who had multiple time points in their analysis were those who had at least two CT images between baseline and death. Images were analyzed using SliceOmatic® V4.2 software with CT image parameters that include: contrast enhanced or unenhanced, 5 mm slice thickness, 120 kVp, and 290 mA. Two adjacent axial scans of the same series were analyzed at each time point and averaged to quantify muscle and adipose tissue cross sectional area, and the mean skeletal MA (HU). CT images are one of the preferred methods for analyzing muscle mass in cancer patients (16) and analysis at the 3rd lumbar vertebra (L3) highly correlates with whole body volumes of muscle and adipose tissue (17). Total muscle (quadratus lumborum, psoas, erector spinae, external obliques, transverse abdominis, internal obliques, and rectus abdominis muscle groups) and adipose tissue (intermuscular, visceral, and subcutaneous) cross-sectional area (cm^2) were calculated as the product of the total number of tissue pixels and pixel surface area.

Muscle area was assessed for the full range of -29 HU to +150 HU which encompasses normal attenuation muscle, ranging from +30 to +150 HU, and reduced attenuation muscle, which includes the areas ranging from 0 to +29 HU and from -29 to 0 HU. Skeletal muscle index (cm^2/m^2) is the muscle cross-sectional area normalized by height. Intermuscular adipose tissue and subcutaneous adipose tissue were each quantified between -190 to -30 HU, and visceral adipose tissue between -150 to -50 HU.

Changes in muscle and adipose tissue cross-sectional area were calculated as the absolute loss or gain of tissue area during each scan interval, and change in MA was evaluated as the absolute change in the mean radiation attenuation between each interval. On a whole-body basis, muscle cross-sectional area change of 6.0 cm^2 is equivalent to a change of 1 kg of skeletal muscle and 14.7 cm^2 total fat cross-sectional area is the equivalence of 1 kg of adipose tissue (17).

2.2.3 Statistics

Data are expressed as mean \pm standard deviation for normally distributed continuous data or as median (interquartile range) for other continuous variables, and as percentages for categorical variables. Student's t-tests were used to compare the mean MA of two groups within a patient characteristic. General linear model regression was used to generate exploratory models for predictors of MA at baseline and predictors of change in MA, both treated as continuous variables. Regression models examined associations with age, muscle and total adipose tissue cross-sectional area as continuous variables, and with sex, and time to death as categorical variables. The reference category for time to death (>92 days to death) was chosen based on previous work which showed a sharp intensification of cancer cachexia during the last 3 months preceding death (4, 18),

as well as trends within the current data (see results section), that illustrate the rapid, exponential decline in the muscle-related parameters cross-sectional area and attenuation within 3 months until death. Cancer diagnosis was examined for variation in MA and was not included in the multivariate analysis as no variation was found. Statistical analysis was conducted using SPSS software version 19.0 (SPSS, Chicago- IL). All p-values were two-sided and results were considered significant at the $p < 0.05$ level.

2.3 Results

2.3.1 Patient characteristics at baseline

Baseline data for 1719 patients are presented in **Table 2-1**. All CT derived descriptors, including muscle cross-sectional area and attenuation and fat cross-sectional area, showed considerable variation. Values for MA ranged from 6.0 to 86.0 HU. **Figure 2-1** illustrates the variability in MA using CT images and compares two similar lung cancer patients (similar age, sex, BMI) at muscles adjacent to the 3rd lumbar vertebra, one with lower MA and the other with higher MA. The patient with higher mean MA (43.5 HU) had 78% of the muscle cross-sectional area in the normal attenuation range. The patient with lower mean MA (18.5 HU) had 37% of the cross-sectional area in the normal attenuation range for muscle.

Results from the linear regression model for predictors of MA are shown in **Table 2-2**. Analysis at both the univariate and multivariate level included the variables: days to death (≤ 92 vs. > 92 days), sex, age (continuous), and cross sectional area of skeletal muscle (continuous) and total adipose tissue (continuous). In the multivariate model, MA was lower with each greater age ($p < 0.001$), males ($p < 0.001$), and a shorter time to death ($p = 0.003$) in comparison with their reference groups. For body composition, MA was

lower in association with lower muscle ($p<0.001$) and higher total adipose tissue cross-sectional area ($p<0.001$).

2.3.2 Change in muscle radiation attenuation over time to death in longitudinal cohort

CT scans are repeated clinically to follow disease progression and response to treatment. The time to death analysis could be completed on patients who had died at the time of this analysis, $n=237$ patients with a total of 835 CT images. Overall changes in mean MA and for mean muscle and fat cross-sectional areas in relation to days to death are illustrated in **Figure 2-2**. Mean change in mean MA and muscle and adipose tissue cross-sectional area across specific time intervals within 1, 3, 6, 9, and 12 months prior to death are shown. The changes were exponential, as loss of mean MA, and muscle and fat cross-sectional increased more rapidly as death approached.

Results for the linear regression model for predictors of change in MA are shown in **Table 2-3**. From the univariate analysis, an increase in total adipose tissue cross-sectional area was a highly significant ($p<0.001$) risk factor for a loss of MA. There was a trend ($p=0.06$) for survival <92 days to predict a loss in MA. Though sex ($p=0.6$) was not a significant predictor of MA change, it was included in the multivariate model with total adipose tissue cross-sectional area and time to death to determine if it would have an effect upon these other variables. At the multivariate level (**Table 2-3**), only total adipose tissue cross-sectional area ($p<0.0001$) and days to death ($p=0.03$) were significant predictors of MA loss.

2.4 Discussion

We assessed characteristics associated with lower MA in patients with cancer at the time they were diagnosed with advanced stage disease and referred to a cancer center for treatment. Initial baseline values were available for 1719 patients, and we also evaluated MA change in 246 patients. Lower baseline MA was associated with increased age, male sex, decreased days to death, lower absolute muscle and higher total adipose tissue cross-sectional areas. Loss of MA during the cancer trajectory was significantly associated with only total adipose tissue cross-sectional area and time to death.

This study has several strengths that have not been present in previous investigations. First, the sample size is much higher than most prior studies on MA in cancer and non-cancer populations. Also, this is the first to attempt to examine MA at a multivariate level, allowing us to identify five independent predictors of MA. These factors (age, sex, fat mass, muscle mass and time to death) were all suggested by prior studies, but their relative magnitude becomes clearer in the multivariate model. For example, MA is a continuous function of fat cross sectional area (positive relationship) and of muscle cross sectional area (negative relationship), and thus the lowest attenuation values were found in sarcopenic obesity. The effect of sex in univariate analyses is potentially confounded in that body composition differs in the 2 sexes (3, 17, 19). Similar to other univariate analyses (9, 20, 21), men had a higher absolute value of MA. However, when other factors were taken into account at the multivariate level, men had significantly lower MA.

There is some variation in the literature in the way in which MA has been defined by prior investigators. Low MA has been defined using cut points detected for an association between MA and mortality (3) using a statistical approach for finding such

cut points called optimal stratification, and this definition was utilized in this study. Another author split a population of patients with melanoma into tertiles according to their psoas MA values and identified very poor survival in the lowest tertile (7). Antoun and coworkers classified low MA as all individuals whose mean MA values could be found below the median MA value for a population of patients with renal cell carcinoma (8).

When MA has a reduced value, it is clear that there is a left-shift in the distribution of attenuation values found within the tissue overall (**Figure 2-1A**.) Thus, the proportion of the tissue cross-sectional area with <30 HU is increased. The term low attenuation muscle has been used to refer to this range. There is some variation in the literature as to how this is defined and we, like others, included the range of -29 to +29 HU (1-4, 8, 19, 23). In comparing our attenuation values to those found in the literature it should be noted that some investigators define low attenuation muscle within the range of 0 to +29 HU (6, 14, 15, 22, 24), and thus do not consider -29 to 0 HU within either the muscle or the intermuscular adipose tissue depots. We feel that this omission is not justified, as for example, 19% of the muscle measured in **Figure 2-1A** was low attenuation muscle in the -29 to 0 HU range, this range should not be excluded. An agreement on the characterization of low MA, and low attenuation muscle, is required in order to meaningfully compare the different features of this phenomenon.

Variables used in this study can explain some but not all of the variation observed in MA. Certain limitations to this study could help to further explain this variation. One of these limitations is the sensitivity of the spiral CT scanner. While all of these images were acquired in the same imaging department, there is some instrument-related variation

to be expected. Another limitation is that comorbidities were not known for patients in this study. Previous studies have illustrated that conditions such as type II diabetes in addition to obesity result in a decrease of as much as 15.3 HU of MA (6, 14, 22, 24). Other decreases in MA due to comorbidities include 3.4 to 9.0 HU due to diseases related to the degeneration of the lumbar vertebrae or spinal stenosis (11, 12), and as much as 13.8 HU in osteoarthritis patients before hip replacement surgery and 10.1 HU after surgery (13). Since we observed that effects of high fat mass could be separated from effects of age, it may be possible that effects of age actually includes independent effects of these specific comorbid conditions. Older cancer patients have been characterized to multiple comorbidities (25). Thus, change in MA will depend upon the influence of numerous other factors. Previous works have not determined whether the effect of age is due to the fact that the patients were older in comparison to the younger population, or on the various comorbidities that may occur in the higher age groups. Cancer progression is evidently independently related to reduced MA, and there was a progressive loss of MA that was most evident in the last few months of life. The cause of this drop in MA has yet to be determined.

Tables

Table 2-1: Characteristics and computed tomography image analysis at baseline for all patients, and advanced cancer patients with multiple scans only

Characteristic	All	Longitudinal Cohort
Patients, n	1719	246
Male %	44	56
Age (years)*	64.2 ± 11.2	61.5 ± 10.1
Median time to death (Range, days)	303 (3261)	92 (3008)
Cancer site, no. (%)		
Colorectal	808 (47)	35 (14)
Respiratory	560 (33)	120 (49)
Pancreas	207 (12)	61 (25)
Stomach	51 (3)	0
Cholangiocarcinoma	30 (2)	30 (12)
Esophageal	24 (1)	0
Other Gastrointestinal†	39 (2)	0
BMI (kg/m ²)*	25.6 ± 5.3	25.5 ± 5.1
SMI (cm ² /m ²)*	47.2 ± 9.5	48.4 ± 9.0
Total L3 muscle CSA (cm ²)*	136.4 ± 34.9	139.4 ± 33.5
Total L3 adipose tissue CSA (cm ²)*	304.2 ± 177.1	306.8 ± 179.4
Mean MA (HU)*	35.2 ± 9.4	35.9 ± 9.4

BMI = Body Mass Index; SMI = Skeletal Muscle Index; L3 = third lumbar vertebra; CSA = Cross Sectional Area; MA = Muscle radiation attenuation; HU = Hounsfield Units

* Mean ± standard deviation

† Other gastrointestinal cancers: digestive tract and accessory organs.

Table 2-2: General linear model regression analysis of muscle radiation attenuation at baseline (continuous variable)

Explanatory Variables	Parameters	Baseline Muscle Radiation Attenuation					
		Univariate			Multivariate		
		Coefficient	95% Confidence Interval	P Value	Coefficient	95% Confidence Interval	P Value
Total L3 muscle CSA (cm ²) <i>(Continuous variable)</i>		0.018	0.002 to 0.034	0.03	0.09	0.07 to 0.11	< 0.001
Total L3 adipose tissue CSA (cm ²) <i>(Continuous variable)</i>		-0.026	-0.029 to -0.024	< 0.001	-0.032	-0.035 to -0.029	< 0.001
Age <i>(Continuous variable)</i>		6.7	5.7 to 7.7	< 0.001	-0.28	-0.32 to -0.24	< 0.001
Sex	Male <i>(vs. Female)</i>	0.3	-0.8 to 1.4	0.6	-2.3	-3.5 to -1.1	< 0.001
Time to death	≤ 92 days <i>(vs. >92 days)</i>	-1.8	-3.5 to -0.2	0.005	-1.9	-3.1 to -0.7	0.003

CSA = Cross Sectional Area; L3 = third lumbar vertebra

Table 2-3: General linear model regression analysis of factors associated with change in muscle radiation attenuation (continuous variable)

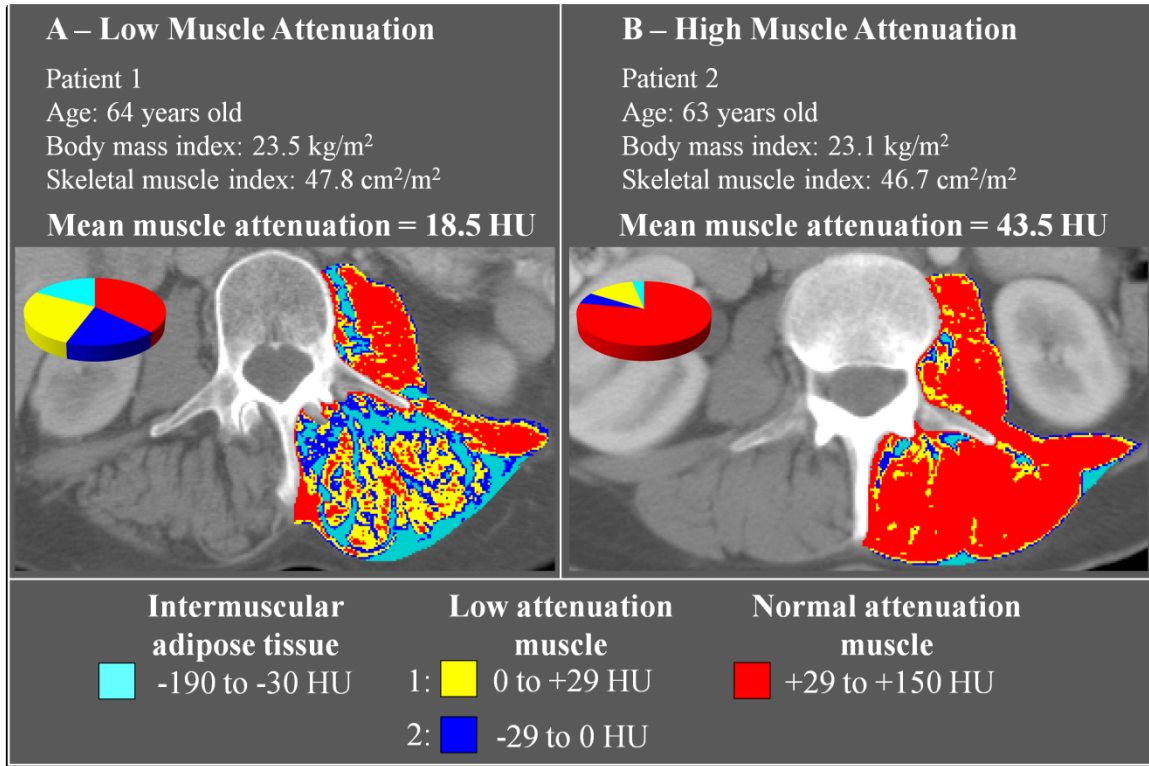
Explanatory Variables	Parameters	Change in Muscle Radiation Attenuation					
		Univariate			Multivariate		
		Coefficient	95% Confidence Interval	P Value	Coefficient	95% Confidence Interval	P Value
Total L3 muscle CSA (cm ²)* (Continuous variable)		-0.01	-0.03 to 0.01	0.3	-	-	-
Total L3 adipose tissue CSA (cm ²) (Continuous variable)		-0.007	-0.011 to -0.003	<0.001	-0.008	-0.012 to -0.004	<0.001
Age* (Continuous variable)		0.03	-0.04 to 0.10	0.3	-	-	-
Sex*	Male (vs. Female)	-0.4	-1.8 to 1.1	0.6	0.3	-1.2 to 1.7	0.7
Time to death	≤ 92 days (vs. >92 days)	-1.4	-2.8 to 0.1	0.06	-1.6	-3.0 to -0.2	0.03

*Was not used in multivariate model due to non-significance

CSA = Cross Sectional Area; L3 = third lumbar vertebra

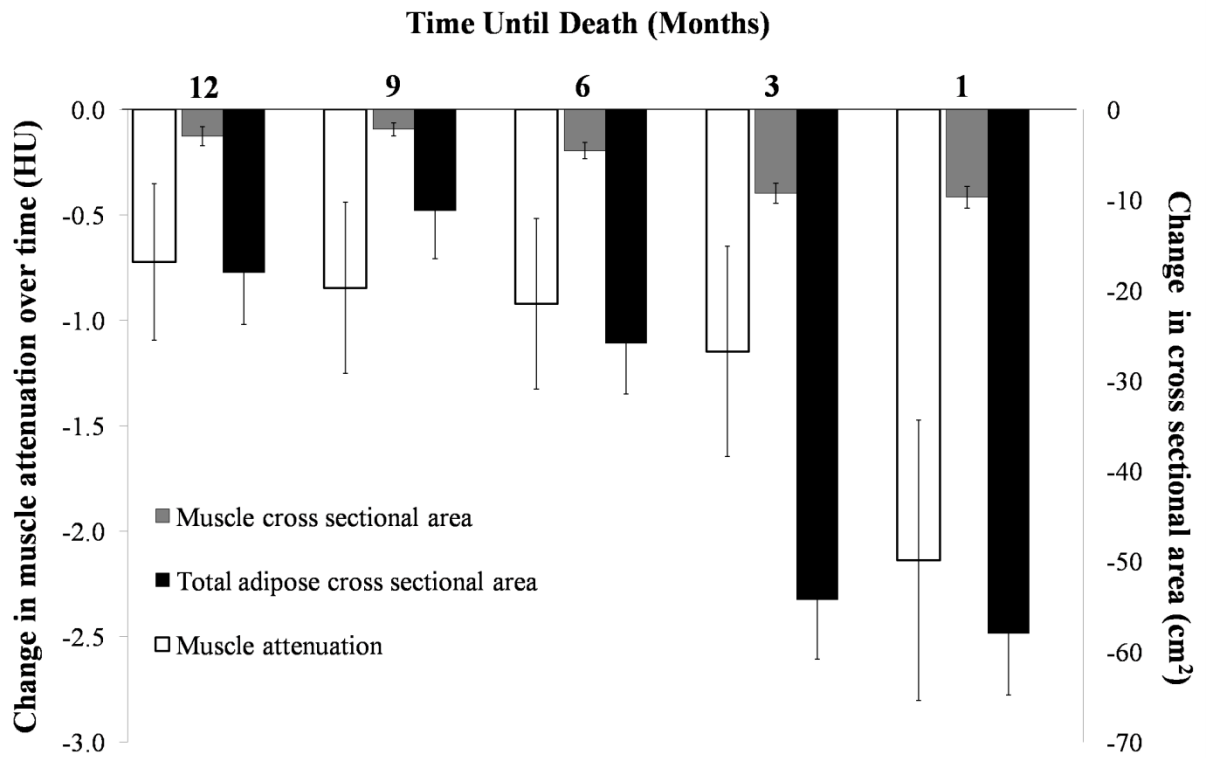
Figures

Figure 2-1: Two lung cancer patients with low (A) and high (B) mean muscle radiation attenuation



Attenuation ranges used for the analysis of normal attenuation (red), low attenuation region 1 (yellow), and low attenuation region 2 (dark blue) muscle, as well as intermuscular adipose tissue (IMAT; teal), are shown. (A) Patient with low muscle radiation attenuation (18.5 HU) had 37% of the cross-sectional area is in the normal attenuation range, 27% of the area is in the low attenuation muscle region 1, 19% of the area is in the lower attenuation muscle region 2, and 17% is IMAT. (B) Patient with high muscle radiation attenuation (43.5 HU) had 78% of the cross-sectional area is in the normal attenuation range, 13% of the area is in the low attenuation muscle region 1, 6% of the area is in the lower attenuation muscle region 2, and 3% is IMAT.

Figure 2-2: Change in muscle radiation attenuation and tissue cross sectional area across months to death



Data points represent mean and standard error of the mean changes; for intervals of patients who were evaluated by computed tomography within muscle radiation attenuation, and muscle and total adipose tissue cross sectional area within 1, 3, 6, 9, and 12 months prior to death (n=32, 177, 168, 101, 138), respectively.

References

1. Prado CM, Lieffers JR, McCargar LJ, et al. Prevalence and clinical implications of sarcopenic obesity in patients with solid tumours of the respiratory and gastrointestinal tracts: a population-based study. *Lancet Oncol* 2008; 9:629-635.
2. Tan BH, Birdsell LA, Martin L, et al. Sarcopenia in an overweight or obese patient is an adverse prognostic factor in pancreatic cancer. *Clin Cancer Res* 2009; 15:6973-6979.
3. Martin L, Birdsell L, MacDonald N, et al. Cancer cachexia in the age of obesity: Skeletal muscle depletion is a powerful prognostic factor, independent of body mass index. *J Clin Oncol* 2013; 31:1539-1547.
4. Prado CMM, Sawyer MB, Ghosh S, et al. Central tenet of cancer cachexia therapy: Do patients with advanced cancer have exploitable anabolic potential? *Am J Clin Nutr* 2013;98:1012-1019.
5. Aubrey J, Esfandiari N, Baracos V, et al. Measurement of skeletal muscle radiation attenuation and basis of its biological variation. *Acta Physiol.* 2014;210(3):489-497.
6. Goodpaster BH, Kelley DE, Thaete FL, et al. Skeletal muscle attenuation determined by computed tomography is associated with skeletal muscle lipid content. *J Appl Physiol* 2000; 89:104-110.
7. Sabel MS, Lee J, Englesbe MJ, et al. Sarcopenia as a prognostic factor among patients with stage III melanoma. *Ann Surg Oncol* 2011; 18(13):3579–3585.
8. Antoun S, Lanoy E, Iacovelli R, et al. Skeletal muscle density predicts prognosis in patients with metastatic renal cell carcinoma treated with targeted therapies. *Cancer* 2013;119:3377-84.

9. Anderson DE, D'Agostino JM, Bruno AG, et al. Variations of CT-based trunk muscle attenuation by age, sex, and specific muscle. *J Gerontol A-Biol Sci Med Sci* 2013; 68:317-323.
10. Taaffe DR, Henwood TR, Nalls MA, et al. Alterations in muscle attenuation following detraining and retraining in resistance-trained older adults. *Gerontol* 2009; 55:217-223.
11. Hicks GE, Simonsick EM, Harris TB, et al. Trunk muscle composition as a predictor of reduced functional capacity in the health, aging and body composition study: The moderating role of back pain. *J Gerontol A-Biol Sci Med Sci* 2005; 60:1420-1424.
12. Hultman G, Nordin M, Saraste H, et al. Body composition, endurance, strength, cross-sectional area, and density of MM erector spinae in men with and without low back pain. *J Spin Disord* 1993; 6:114-123.
13. Rasch A, Bystrom AH, Dalen N, et al. Persisting muscle atrophy two years after replacement of the hip. *J Bone Joint Surg Br* 2009; 91:583-588.
14. Lee S, Kuk JL, Davidson LE, et al. Exercise without weight loss is an effective strategy for obesity reduction in obese individuals with and without type 2 diabetes. *J Appl Physiol* 2005; 99:1220-25.
15. Poehlman ET, Dvorak RV, DeNino WF, et al. Effects of resistance training and endurance training on insulin sensitivity in nonobese, young women: A controlled randomized trial. *J Clin Endocrin Metab* 2000; 85: 2463-68.
16. Fearon K, Strasser F, Anker SD, et al. Definition and classification of cancer cachexia: An international consensus framework. *Lancet Oncol* 2010; 12: 489- 495.

17. Shen W, Punyanitya M, Wang Z, et al. Total body skeletal muscle and adipose tissue volumes: Estimation from a single abdominal cross-sectional image. *J Appl Physiol* 2004; 97:2333-2338.
18. Lieffers JR, Mourtzakis M, Hall, KD, et al. A viscerally driven cachexia syndrome in patients with advanced colorectal cancer: contributions of organ and tumor mass to whole-body energy demands. *Am J Clin Nutr* 2009; 89: 1173-1179.
19. Baracos VE, Reiman T, Mourtzakis M, et al. Body composition in patients with non-small cell lung cancer: a contemporary view of cancer cachexia with the use of computed tomography image analysis. *Am J Clin Nutr* 2010; 91(4):1133S–1137S.
20. Goodpaster BH, Carlson CL, Visser M, et al. Attenuation of skeletal muscle and strength in the elderly: The health ABC study. *J Appl Physiol* 2001; 90:2157-2165.
21. Kalichman L, Hodges P, Li L, et al. Changes in paraspinal muscles and their association with low back pain and spinal degeneration: CT study. *Eur Spine J* 2010; 19:1136-1144.
22. Goodpaster BH, Thaete FL, Kelley DE. Thigh adipose tissue distribution is associated with insulin resistance in obesity and in type 2 diabetes mellitus. *Am J Clin Nutr* 2000; 71(4): 885-855592.
23. Tandon P, Ney M, Irwin I, et al. Severe muscle depletion in patients on the liver transplant wait list: its prevalence and independent prognostic value. *Liver Transplant* 2012; 18(10): 1209–1216.
24. Kelley DE, McKolanis TM, Hegazi RA, et al. Fatty liver in type 2 diabetes mellitus: Relation to regional adiposity, fatty acids, and insulin resistance. *Am J Physiol Endocrinol Metab* 2003; 285(4): E906-916.

25. Lieffers JR, Baracos VE, Winget M, et al. A comparison of Charlson and Elixhauser comorbidity measures to predict colorectal cancer survival using administrative health data. *Cancer* 2011; 117(9): 1957-1965.

CHAPTER 3: Exploratory analyses of human muscle biopsies provide evidence of atrophy and fat infiltration in cancer-associated muscle wasting

3.1 Introduction

Complete assessment of skeletal muscle can be done through exploration of the tissue at multiple levels: cellular, tissue, or whole body. In cancer, absolute measurements of skeletal muscle (1) and depletion of skeletal muscle over time (2) has been documented using computed tomography (CT) imaging. Most research on cancer associated muscle wasting has been done in experimental animal models and already this numbers ~500 papers. In contrast, at this time there have been less than 20 publications examining biopsied human muscle from cancer patients.

Several types of stem cells found in skeletal muscle have been proposed to contribute to myogenesis based upon animal models (3-6). However, since most stem cell populations have not been investigated in humans, developmental lineages and interactions between cell types is not well understood. Two stem cell populations supported by human studies include satellite cells (SCs) and multipotent progenitors (3, 7), a group of stem cells that have the capacity to differentiate into adipogenic or myogenic progenitors. Though satellite cells are believed to be the primary contributors to muscle regeneration and repair, only one group has investigated their roles in cancer associated muscle wasting (8). However, this research group used weight loss and IgG (a marker for muscle damage) as the criteria for muscle wasting rather than assessment of skeletal muscle area or mass. In addition, they used the marker Pax7 to identify SCs, which is a protein that can be found in SCs at different stages of its myogenic program (**Figure 3-1A**). In patients with muscular dystrophy (8), multipotent progenitors were

reported to lose the expression of either the marker CD15 or CD56 (**Figure 3-1B**) to become either myogenic or adipogenic, respectively. In patients with muscular dystrophy, Pisani et al. observed significantly greater populations of multipotent progenitors and their adipogenic subpopulations (8). These groups of cells may be of particular interest in the realm of muscle wasting, as one of its distinct features is believed to include infiltration of fat within the muscle.

Fatty infiltration, along with several other structural alterations of skeletal muscle, such as diminished myofibre size (atrophy), increased number of central nuclei, and infiltration of immune cells, may be expected upon examination of the morphology of muscle from individuals with muscle wasting (9). However, morphological analysis of muscle from cancer patients is limited (**Table 3-1**). There is some evidence that muscle fiber sizes are smaller in cancer cachexia than in a control group of healthy volunteers matched for age, sex and height (10). There is also evidence that the presence of centralized nuclei (nuclei within the geometric centre of muscle fibres) as well as internal nuclei (nuclei just within the sarcolemma of the muscle fibres) is greater in patients with newly diagnosed colorectal cancer in comparison to non-cancer controls (11). Otherwise, more recent investigations of muscle biopsies have been limited to the ultrastructure of skeletal muscle using electron microscopy (8, 12). Stephens et al. observed that muscle biopsies from cancer patients contained greater intramyocellular lipid droplets both in number and size compared with control muscle biopsies (12). Similarly, He et al. (8) observed that muscle biopsies from cancer patients showed greater muscle damage, in terms of alterations to the membrane and damage to the overall myofibre, than control biopsies, though this was done on a small portion of the biopsy using electron

microscopy. In both of these studies, patients were designated as being affected by cachexia based on degree of weight loss. However, as weight loss does not necessarily indicate muscle loss, measurements of absolute skeletal muscle mass or change in the tissue over time would have strengthened the validity of their findings. Electron microscopy works under extremely high magnifications, thus both of these investigations examined skeletal muscle in a very narrow point of reference. Histological and immunohistochemical analyses would have complemented both of these studies in determining the overall structure of the muscle, and may provide some support in the investigation of stem cell activity in skeletal muscle.

Past literature attempting to isolate or quantify different cell populations from human skeletal muscle, specifically satellite cells, have used several methods ranging from cell culture, flow cytometry, and immunofluorescence (13-15). However, there has never been an attempt to quantify adipocytes from skeletal muscle in either human or animal models. The idea that muscle of cancer patients is infiltrated by fat comes from relatively recent radiological findings, and very little is known about this from any patient population or experimental system. One objective was to establish a protocol that could isolate both mononuclear cells (MNCs), which include myocytes, stem cells, and immune cells, and adipocytes from a single muscle biopsy. Further analysis of MNCs aids in determining proportions of myogenic and adipogenic cells in patients with differing skeletal muscle characteristics. Evaluations of other parts of the same biopsy as well as CT images provide a more complete understanding of properties of skeletal muscle. Examining these characteristics of skeletal muscle wasting contributes to an unexplored area of research in the cancer setting. Based upon a review of literature regarding stem

cells in non-cancer populations, it is expected that patients with muscle depletion will have a lower number of myogenic stem cells and a greater number of adipogenic stem cells.

3.2 Methods

3.2.1 Muscle biopsies

Intraoperative muscle samples were acquired from either the rectus abdominis (RA, n=26) or sternocleidomastoid (n=2) muscles of surgical patients. Patients with cancer (n=26) had stages II-IV gastrointestinal cancer patients and patients with non-malignant conditions (n=2) such as diverticulitis were recruited from the University of Alberta Hospital. This study was approved by the Alberta Cancer Research Ethics Board. All patients were informed of the potential risks associated with the process of acquiring the muscle specimen and gave written informed consent to participate. Of the 28 patients overall, 19 patients had biopsies collected for the development of a cell isolation protocol, and some were also included in lipid and myosin heavy chain analyses if tissue was available. Biopsies for 7 male cancer patients (including one of the 19 previous patients) were sampled for analysis. Portions of these biopsies were used fresh for flow cytometry analysis and the other portions were sampled for frozen sections to be assessed using light microscopy, biochemical analyses (Appendix A1), and immunofluorescence. One part of the biopsies was transferred in saline-soaked gauze, oriented, and frozen in isopentane cooled in liquid nitrogen, to be sectioned (10 μ m) and processed for histology and immunohistochemistry. The other part of the biopsies was transferred in a sterile culture medium (DMEM Ham's /F-12, (L)-glutamine, 1% penicillin + streptomycin, and calcium chloride) with 20% fetal bovine serum (FBS) on ice to the laboratory within 1

hour. The samples were weighed such that 150 ± 0.5 mg of the tissues were used to isolate mononuclear cells, adipocytes, and other cell populations. Any unused skeletal muscle was frozen directly in liquid nitrogen.

3.2.2 Cell isolation

MNCs were isolated using methods similar to those previously described (15). The following outlines the isolation procedure as it was done for patients 2 and 3, and **Table 3-2** indicates the changes made to the protocol for subsequent biopsies. A 150 mg piece of the biopsy was minced for 1 min (this time increased to ensure that the tissue was thoroughly minced from patient 10 onwards). It was then enzymatically digested by adding 450 μ L of a collagenase-dispase solution (10 mg/mL collagenase I, Gibco/Invitrogen + 2.4 U/mL Dispase II, Gibco/Invitrogen) made in sterile culture medium, and incubated for 10 min at 37°C (5% CO₂). The mixture was agitated after incubation, and 260 μ L of the collagenase-dispase solution was added followed by another incubation period of 10 min at 37°C (5% CO₂). The digested sample was filtered through a 70 μ m mesh into a sterile Petri dish. The mesh was washed with 710 μ L of sterile culture medium containing 20% FBS (equal to the volume of enzyme solution used). The solution was transferred to a centrifuge tube, vortexed for 10 sec, and centrifuged for 10 minutes at 200 x g. The top 100 μ L layer of the supernatant (the layer containing adipocytes) was transferred to a separate tube for adipocyte count under a haemocytometer. For patients 6-19, 100 μ L of the supernatant layers were sequentially removed and transferred to new centrifuge tubes, where 20 μ L of the layers were removed for counting. The remaining layers were replaced in the original tube, which was vortexed for 10 seconds, then centrifuged at 800 x g for 5 min. The pellet

(containing MNCs) was resuspended in 1 mL of phosphate buffered saline (PBS). A small volume of the suspension was mixed in equal volume with trypan blue (1:1), and the solution was triturated. 20 μ L of the solution was transferred to a haemocytometer, and cells were counted. The isolation for some of the biopsies also included a redigestion of the filtrate remaining on top of the 70 μ m mesh after the filtration of the cell suspension. This was done to quantify any remaining MNCs that were not isolated from the first digestion (i.e. not found in the original pellet). Redigestion of the filtrate involved another 2x10 min incubation of the cell suspensions at 37°C (5% CO₂) with the same collagenase-dispase solution used during the first digestion step, a wash with the sterile culture medium with 20% FBS, filtration through a 70 μ m mesh, and centrifugation at 800 x g for 5 min. Cells were also counted using a haemocytometer. Isolation procedures for patients 6-16 included the addition of a red blood cell (RBC) lysis buffer.

3.2.3 Flow cytometry

The remainder of the cell suspension was aliquoted evenly into pre-conditioned tubes such that each tube would contain at least 500,000 cells. As the antibodies used label antigens that are both on the cell surface and within the cell nucleus, three groups of tubes (or wells) were used for different cell antigen types (**Table 3-3**). The tubes were spun again at 800xg for 5 minutes, and the supernatant was removed. The appropriate concentration of the labeled, cell surface primary antibodies were added to their respective tubes and incubated in the fridge for 30-45 minutes. Suspensions were washed with PBS solution, centrifuged again at 800xg for 5 minutes, and the supernatant was decanted. All wells used for analysis were fixed in 100 μ L of 1% paraformaldehyde for

10 minutes at room temperature. After being washed, wells with cell surface antigens only were then refrigerated until cells could be acquired using flow cytometry analysis. All other cell pellets were permeabilized with 0.5% Triton-X in PBS for 15 minutes at room temperature, washed, and incubated with primary, intracellular antigens for 30-45 minutes. Incubation was again conducted if wells required secondary antibody. All remaining wells were then refrigerated until analysis. Wells used for the identification of cells within the multipotent progenitor and satellite cell populations used the antibodies CD34/PE, CD56/APC, CD15/FITC (eBiosciences, 12-0349-42, 17-0567-42, and 11-0159-42, respectively), Pax7/FITC (Developmental Studies Hybridoma Bank), Pax3 (R&D Systems, IC2457A), and MyoD (Abcam, ab126726). The secondary antibody Alexa Fluor 594 (Invitrogen, A-11037) was used for labeling the MyoD primary antibody. Flow cytometry was conducted using the BD Fortessa flow analyzer (BD Biosciences), and programs for analysis included BD FACS Diva and FCS Express 4.

3.2.4 Histology

Frozen sections for haematoxylin and eosin (H&E) staining were placed in Harris' Haematoxylin for 3 min, and then rinsed with distilled water. Sections were immersed in Eosin for 2 minutes and again rinsed under tap water to remove excess stains. The staining was dehydrated with alcohol and then cleared in two changes of xylene. Sections were then mounted with Entellan (Millipore). Frozen sections for Oil Red O (ORO) staining were air dried for 5 minutes, then fixed with 10% neutral buffer formalin for 10 minutes. The sections underwent a sequential rinsing involved two changes of distilled water (2 minutes each), 50% propylene glycol (2 minutes each), and 100% propylene glycol (3 minutes each). Sections were stained with ORO for 20 minutes on an automatic

shaker then rinsed again with one change of 100%, 85%, and 50% propylene glycol (each for 3 minutes). The sections were rinsed in distilled water for 3 minutes, and any excess water was allowed to drain from the sections but not to dry before mounting with Geltol (Sigma Aldrich), rinsed, and mounted. Histological and immunohistochemical slides were visualized with a light microscope and analyzed with ImageJ software (National Institutes of Health [NIH], Washington DC, WA, USA). The average number of myofibres (without artifacts such as tears or folding of the myofibre) measured for myofibre cross sectional area (MCSA) and Feret's diameter (the longest distance between two points, measuring the diameter of irregularly shaped cells) were 145 ± 54 myofibres. Relative amounts of intramyocellular lipids and intermuscular adipocytes in ORO stained sections were marked by an experienced muscle pathologist who was blinded to the status of each patient, as mild (+), moderate (++), and severe (+++), shown in **Figure 3-2**.

3.2.5 Immunofluorescence

Frozen sections were dried for 30 minutes at 37°C before being rinsed in a reaction buffer (Ventana, 950-300) for 5 minutes. The primary antibodies CD34/PE, CD56/APC, and CD15/FITC (eBiosciences, 12-0349-42, 17-0567-42, and 11-0159-42, respectively) were then applied for 30 minutes, and the sections were rinsed again three times with the reaction buffer. An Alexa Fluor 594 (Invitrogen, A-11037) secondary antibody was used for MyoD only for 30 minutes. After the sections were again rinsed three times with the reaction buffer, the slides were dried and covered with a coverslip and refrigerated before viewing. Slides were visualized using a Zeiss LSM710 laser scanning confocal microscope and images were captured using Zen (Zeiss) software.

3.2.6 Myosin heavy chain analysis

Frozen skeletal muscle tissue pieces reserved for myosin heavy chain (MHC) analysis were weighed (25.6 ± 0.9 g) and ground. Ice-cold extraction buffer containing 100 mM $\text{Na}_4\text{P}_2\text{O}_7$, 5 mM EGTA, 5mM MgCl_2 , 0.3 mM KCl and 10 mM Dithiotreitol (ICN Biomedicals) as well as a protease inhibitor (Complete, Roche Diagnostics) was added and mixed with the frozen powder muscle. Mixtures were centrifuged at $12000 \times g$ for 10 minutes at 4°C , and supernatants were transferred to be diluted 1:1 with 100% glycerol and kept at -20°C until analyzed. Before analysis, mixtures were diluted with a modified Laemmli-Lyse Buffer to a concentration of $0.1 \mu\text{g}/\mu\text{L}$ and boiled for 5-10 minutes. Samples were electrophoresed (protein load of $0.75 \mu\text{g}$ per lane, 275 V for 24 hours at 8°C) in duplicate on 10% SDS-PAGE gels. Gels were fixed for 30 minutes in 50% methanol/ H_2O at room temperature. MHC isoforms were then detected using an ammoniacal silver solution and analyzed by densitometry, and are expressed as percentages.

3.2.7 Lipid analysis

Frozen skeletal muscle tissue pieces reserved for lipid analysis were weighed (50.6 ± 2.0 mg) and ground to be prepared with a chloroform-methanol solution. Beads were added to the bottom of the homogenizer tubes, with samples and 0.8mL of 0.025% CaCl_2 added on top. Samples were homogenized in 20 second intervals for a total of 1 minute. After homogenization, samples were transferred to medium glass tubes and another 0.8 mL 0.025% CaCl_2 was added with 8 mL chloroform-methanol solution. After vortexing, tubes were flushed with nitrogen and refrigerated overnight to separate the liquids. The clearest layer at the bottom of the tubes containing the lipids was transferred

to clean methylation tubes the next day and the previous tubes were washed and allowed to settle for the lipids to separate once again. The sample tubes with the clean lipid layer were dried under nitrogen gas. Each G plate was spotted with a standard and with a sample mixture (in duplicate) and kept in the solvent mixture tank until the solvents reached 0.5 cm from the top of the plate. After drying the G plates, ultraviolet light was used to identify the phospholipid and triglyceride bands, which were scraped into separate tubes. A standard (C15:0, 10.2 µg/100 mL hexane) was added to enable quantification. Triglyceride tubes were prepared in potassium hydroxide and heated on a dry bath for one hour. Hexane was added to both triglyceride and phospholipid tubes and both were heated for another hour. Samples were transferred to their respective inserts until analyzed by gas chromatography. Gas chromatography with flame ionization detector (GC-FID) analysis was used for fatty acid extractions using an Agilent 7890A instrument. Methylated samples (1.5 µL each) were injected onto a 30 m x 0.25 mm ID BP20 column and a 0.25 µm film thickness (SGE Analytical Science). A split flow injection to the gas chromatography column set to 15 was used and the initial temperature of the inlet maintained at 275°C. The gas chromatography run parameters were: initial temperature set to 150°C and maintained for 1 minute, then increased at a rate of 5°/minute to a temperature of 180°C. The temperature ramp rate was then slowed to 2°/minute until a temperature of 225°C was reached and maintained for 5 minutes. The temperature was then quickly raised by 80°/minute to 245°C and maintained for 3 minutes. Identification of sample fatty acids in was achieved by comparing retention times to that of a standard methylated fatty acid mixture (GLC461, Nu-chek Prep Inc., Elysian, USA). Quantitative data was obtained by comparing the GC-FID response for

each fatty acid to a known amount of C17:0 internal standard. A commercially available standard of known composition based on C15:0 was used to identify sample fatty acids.

Total triglyceride measurements were done as μg per gram of skeletal muscle ($\mu\text{g/g}$).

3.2.8 Computed tomography image analysis

Skeletal muscle in CT images was quantitatively analyzed at the 3rd lumbar vertebra (L3) for total muscle and adipose tissue cross sectional area (CSA; cm^2) (SliceOmatic® V4.2 software). Skeletal muscle index (SMI; cm^2/m^2) is the CSA normalized by height. Intermuscular adipose tissue (IMAT) was quantified between -190 to -30 HU, visceral adipose tissue between -150 to -50 HU, and subcutaneous adipose tissue between -190 to -30 HU. Muscle area was assessed as the range between -29 HU to +150 HU and the mean muscle radiation attenuation, believed to be indicative of lipids within the muscle, for all pixels was also measured. The skeletal muscle was analyzed as a total of RA, internal and external obliques, transversus abdominis, psoas, quadratus lumborum, and erector spinae muscles. RA muscles were also analyzed separately for CSA, mean attenuation, and any IMAT that may be present within the RA. Sarcopenic status for seven male cancer patients determined based on previous cutpoints (16). Patients with body mass index $>25 \text{ kg/m}^2$ and SMI $<53 \text{ cm}^2/\text{m}^2$ and patients with body mass index $<25 \text{ kg/m}^2$ and SMI $<43 \text{ cm}^2/\text{m}^2$ were considered to be sarcopenic.

3.3 Results

3.3.1 Development of cell isolation protocol

Nineteen biopsies were collected to develop the protocol for the simultaneous isolation of fat and mononuclear cells. Several changes were made to the original procedure due to inconsistencies in cell yield. Though the procedure provided a cell count

for both adipocytes and MNCs for patients 2 (20,000 and 2.43 million, respectively) and 3 (60,000 and 4.59 million, respectively), subsequent attempts resulted in a low (20,000 cells for both adipocytes and MNCs) or no cell yield (**Table 3-4**). The counts increased once again with the addition of calcium chloride to the enzyme solution. Other changes included an increase in the volume of the collagenase-dispase solution used as well as the corresponding volume of the culture medium with 20% FBS wash. Despite these changes, cell counts continued to be inconsistent between the biopsies analyzed. The next alteration was the pre-warming of the enzyme and wash solutions, which resulted in more consistent yields of MNCs, if not for adipocytes, for each muscle biopsy. For the biopsies from which multiple layers were removed for adipocyte counting, cells could be found in more than one layer, and were not always in the top layer.

It was also discovered that the RBC lysis buffers used had a negative effect on the MNC count. After addition of the lysis buffers, only 1-9% of all cells would remain in the cell suspensions. A larger portion of cells remained in only one case (patient 12, 62%) after the lysis buffer was added. Therefore, for the remaining patients, RBC lysis buffer was not used.

3.3.2 Radiological characteristics of skeletal muscle of patients who consented to biopsy represent the distribution seen in larger cohorts of cancer patients

Of 28 patients biopsied, CT images could be acquired for analysis for 20 patients. The median number of days between the date of muscle biopsy acquisition and the CT image date was 39.5 ± 13.7 days. The mean muscle CSA and mean muscle radiation attenuation of male patients were 161.9 ± 8.4 cm² and 32.1 ± 11.3 respectively, and for women was 105.7 ± 23.8 and 31.0 ± 10.3 , respectively. In terms of adipose tissue,

average CSA for intermuscular adipose was $14.5 \pm 16.3 \text{ cm}^2$, for visceral $149.2 \pm 116.9 \text{ cm}^2$, and for subcutaneous $191.4 \pm 122.4 \text{ cm}^2$. The muscle area and attenuation of these patients can be placed into context against a larger cohort of male lung and gastrointestinal cancer patients (n=370). This is illustrated in **Figure 3-3**, where the twenty patients are located along the entire distribution, and demonstrate that they are representative of a larger population of patients. Six patients have a greater muscle CSA and five patients have greater muscle radiation attenuation on average than the cohort of patients. **Figure 3-4** reflects that overall, the patients have lower CSA and attenuation. This indicates that at the tissue and cellular levels, it would be expected that there would be atrophy of the myofibres and altered activity of myogenic stem cells contributing to the low muscle CSA. Similarly, for the low muscle radiation attenuation, tissue and cellular characteristics can be explored to determine if there is excessively fatty muscle and altered adipogenic stem cell activity.

3.3.3 Morphological analyses of muscle tissue sections

Seven of the muscle biopsies provided were sectioned to explore structural and stem cell properties of skeletal muscle in male cancer patients (**Table 3-5**). These properties allowed a preliminary profile of the patients. The average muscle CSA and mean muscle radiation attenuation of these seven patients were $163.3 \pm 39.5 \text{ cm}^2$ and $32.6 \pm 14.6 \text{ HU}$. Three of 7 patients (42.9%) were sarcopenic. The average muscle CSA and mean muscle radiation attenuation of the RA muscle alone for these patients was $14.1 \pm 3.6 \text{ cm}^2$ and $23.1 \pm 16.4 \text{ HU}$. Patients 14 and 24, two male cancer patients of identical age, were selected as illustrations as they represented the extremes (circled points in **Figure 3-4**) of patients within this data set (**Table 3-6**). The extent to which these

patients differ based on their radiological characteristics is illustrated in their CT images (**Figure 3-5**). Patient 24 was not sarcopenic and had a high muscle CSA and the highest mean muscle radiation attenuation (175.7 cm^2 and 54.4 HU) of any patient in the cohort. Patient 14 was sarcopenic and had both the lowest skeletal muscle CSA and muscle radiation attenuation (109.0 cm^2 and 7.1 HU , respectively). An accompanying difference between these patients was the adipose tissue CSA, particularly IMAT, which was 75.0 cm^2 for P14 and 4.1 cm^2 for P24. Of the patients with MHC analysis completed for their muscle biopsies, this patient was also observed to have the greatest proportion of type I (72.1%) in comparison to type II (27.9%) muscle fibres. These values can be contrasted to patient P24 who had a higher proportion of total type II muscle fibres (64.2%). The MCSA and diameter for patient P14 ($5758 \pm 3117 \mu\text{m}^2$ and $119 \pm 37 \mu\text{m}$, respectively) and P24 ($5026 \pm 2156 \mu\text{m}^2$ and $108 \pm 24 \mu\text{m}$) are approximately the same. However, the variation in myofibre sizes in P14 was greater (**Figure 3-6C, E**) than P24 (**Figure 3-6D, F**) with some very small myofibres present (i.e. 15% percent of myofibres were less than $2000 \mu\text{m}^2$ in P14 as opposed to 1% in P24). Myofibres in both patients P14 (68% of myofibres counted) and P24 (10% of myofibres counted) contained centrally located nuclei (**Figure 3-6A, B**) indicating regeneration. However, patient P14 also exhibited some pyknotic nuclei as well as myofibres that were triangular in shape, suggesting denervation of the muscle fibres. Muscle sections stained with H&E and ORO from both patients displayed both intermuscular adipocytes (**Figure 3-7A-D**) and lipid droplets (**Figure 3-7 E, F**) within the muscle, though this was observed to be greater in P14. This fatty infiltration is reflected in the total amount of triglycerides measured for patient P14 ($25475.1 \mu\text{g/g}$) in comparison to P24 ($4143.8 \mu\text{g/g}$). These values also fall at the

extremes of a triglyceride distribution (**Figure 3-7G**) from a larger data set of male cancer patients (n=42). For those patients who had lipid extraction from muscle for analysis, fatty acid profiles (saturated, unsaturated, n-3, n-6) did not appear to show inter – individual variation.

3.3.4 Stem cell populations in muscle wasting: preliminary data

For all patients with stem cell data, analysis of multipotent progenitors and their subpopulations based on immunofluorescence and flow cytometry did not show the same absolute numbers of multipotent, myogenic, and adipogenic progenitors, though they did tend to provide similar proportions relative to each other (**Table 3-5**). The average percentages of MNCs determined through immunofluorescence (**Figure 3-8**) to be multipotent (CD56+CD34+CD15+), myogenic (CD34+CD56+CD15-), and adipogenic (CD34+CD56-CD15+) were $1.33 \pm 0.63\%$, $1.13 \pm 0.74\%$, and $1.31 \pm 0.82\%$, respectively (n=7). Overall, P14 has less than half the total multipotent, myogenic, and adipogenic progenitors (3.49%) than P24 (7.47%). On average, patient P14 had a lower and patient P24 had a higher percentage of multipotent progenitors (0.52% and 2.24%). In patient P14, there were more myogenic and adipogenic progenitors than multipotent progenitors, while in P24, proportions of these populations were approximately the same.

3.4 Discussion

These investigations provide an initial, comprehensive data set on muscle biopsies in cancer cachexia by incorporating radiological data with morphological and biological characteristics. The radiological characteristics have been acquired using methods that have been developed and used across larger populations (1), against which the sample used here for biopsy can be framed (16). This allows any patient with a CT scan, measure

of height, and muscle characterizations (including CSA, attenuation, and change over time if serial scans are available) to be placed in context of the population from which they were derived. This current research includes key methodological developments for the acquisition, processing, and evaluation of muscle biopsies, with a focus on morphology and isolation of cell populations. Due to the delicate nature of adipocytes, their isolation alongside MNCs required some technical considerations such as correct temperatures and centrifugation settings to prevent rupture of the cells. In addition, correct fixation and permeabilization conditions were required for processing of satellite cells for flow cytometry, as the analysis for this population of cells is not normally conducted using multiple antibodies, especially those including antibodies against both cell surface and nuclear antigens, within one well. Thus, in this study, a clearly defined protocol for the assessment of cell populations by flow cytometry and immunofluorescence has been established. Though all analyses were not done for all patients, based upon the preliminary evidence presented, the degree of variation of the parameters measured emphasizes the significance of creating a skeletal muscle profile, i.e. identifying the position of each patient on the distributions of a variety of muscle features. This will continue to provide an idea of sample size considerations in future investigations.

Each one of the cancer patients represented here by a biopsy was characterized based on CT image analysis. Within populations of cancer patients the difference between the least muscular and the most muscular individuals is more than twofold in total lumbar muscle CSA. Severe skeletal muscle depletion, known as sarcopenia, was present in approximately half of the sampled patients. Likewise, cutpoints for reduced

muscle radiation attenuation, also associated with enhanced chemotherapy toxicity and decreased survival have been defined in the literature (17), and patients within our sample also showed reduced muscle radiation attenuation to varying degrees. This investigation is the first to evaluate patients by CT, as compared to prior investigations where patients were classified according to degree of weight loss but without any specific indication of muscle loss (8, 12). We suggest that all patients whose biopsies go on to be used for specific biochemical morphological and other analyses, be quantified for 2 key parameters, muscle cross-sectional area, muscle radiation attenuation and if available rates of muscle loss or gain, from repeated scans over time.

In this exploratory study we sought to optimize methodology and to identify specific indices of biological alteration within the muscle cell populations. This included analysis of a small sample, for a series of features indicated in appendix number A1. Two specific patients were chosen to illustrate the extremes of muscle phenotype in cancer patients; one of these had above average muscle area and attenuation and therefore more normal muscle where the other was extremely sarcopenic with extremely low attenuation values. Average myofibre size across the evaluated sample did not appear to vary much between individuals, however the 3 patients with the lowest muscle cross-sectional area including patient P14 had a high standard deviation of myofibrillar cross-sectional area and hence a significant number of extremely small fibres. There were other pathological changes in some myofibres including centrally located nuclei. Very small myofibres and centrally located nuclei have been noted in a variety of dystrophies, myopathies, and other conditions with muscle wasting such as chronic obstructive pulmonary disease (18, 19, 20). Also, the MHC analyses provided for three of the

patients revealed some differences in the proportion of type I and type II myofibres of patient P14 and patients P24 and P26, who had a higher muscle CSA and attenuation. Research in animal models suggests preferential loss of fast fibres (21) in cancer cachexia and the absence of detectable type IIX myosin heavy chains in patient 14 would be consistent with that. However, it should be noted that cancer-associated muscle wasting in humans is its own phenomenon; comparisons with other conditions, and particularly comparisons of humans with animal models, has limitations and future analyses must be done to validate the findings presented here. The fibre type most likely to atrophy in this population of patients can be confirmed in the future through muscle fibre type analyses, such as immunohistochemical ATPase stains and the use of monoclonal antibodies in immunohistochemistry.

Mean radiation attenuation of muscle from healthy young adults is approximately 50 Hounsfield units. Several recent publications with large data sets indicate that the mean attenuation of muscle from cancer patients is typically around 32 HU with a standard deviation of about 10 HU (16, 22). Several patients in our sample had large cross-sectional areas of intramuscular adipose tissue, as well as mean attenuation values as low as 7 HU, suggesting fatty infiltration is an important constituent of cancer associated muscle wasting. So far this has been evaluated in only a single published work, which was conducted at electron microscope level and showed increased levels of intramyocellular lipid in patients with cancer associated weight loss compared with healthy controls (12). The present study illuminates further aspects of fatty infiltration, noting some patients had high total tissue triglyceride and fatty acid levels, morphologically distinct regions containing large tracts of adipocytes evident in H&E

stained sections and confirmed to have high lipid content using staining with ORO. From both the presence of excess adipocytes and lipid droplets in histological analyses and the differences in triglyceride values, increased fatty infiltration is a noteworthy contributor to lower muscle radiation attenuation values. Identifying the source of excess fat as either adipocytes or lipid droplets could be significant in the occurrence of fat infiltration within muscle. The presence of adipocytes implies a contribution of local adipogenic precursors. Triglyceride fatty acid content, ranging from 124 to 44117 $\mu\text{g/g}$ tissue (**Table 3-7G**, unpublished data, Aubrey, Putman, Mazurak), can provide a quantification of all fat, where normal estimates of triglyceride content determined from vastus lateralis muscle of lean and obese men range from 9000 to 10000 $\mu\text{g/g}$ (23). However, to determine the difference in the number of adipocytes in a piece of tissue, cell counts taken during the cell isolation protocol may be used. Cell counts done on biopsies in this investigation found 0 to 504000 adipocytes in 150 mg of skeletal muscle. This is confirmed in the histological staining of muscle sections for H&E and ORO, which revealed large clusters of adipocytes. With an established protocol for cell isolation from skeletal muscle, prospective analyses of muscle biopsies can continue to include cell counts to provide further evidence of adipocytes. Patient 14 in particular appears to fit the current idea of fatty infiltration in muscle wasting, as the mean muscle radiation attenuation value derived from CT image analysis was the lowest of all patients, but IMAT and triglyceride content was the highest. These results are in agreement with other studies indicating that fatty infiltration measured in CT images by IMAT and mean muscle radiation attenuation are indicative of the lipid content in muscle (24, 25, 26).

Two sets of observations made in this preliminary investigation fuel interest in further study of stem cell populations in cancer associated muscle wasting. Several lines of evidence suggests possible loss of myogenic potential (wasting, fiber atrophy) and possibly concurrent gain of adipogenic potential (specifically, increased number of adipocytes). Despite variation in the number of multipotent, myogenic, and adipogenic progenitor populations, there appears to be a pool of these cells maintained in proportions specific to the conditions of the muscle. A previous examination of these populations identified patients with muscular dystrophy to have a greater number of multipotent and adipogenic progenitors than healthy subjects (7). Though deposition of fat has been recognized as a characteristic in both dystrophy and cancer associated muscle wasting, muscle profiles of patients provide an insight as to whether fatty infiltration is indeed occurring in these patients. Patient P24 had a higher percentage of the sum of multipotent progenitors and its myogenic and adipogenic subpopulations than P14 (7.47% and 3.49%, respectively). This could indicate that the muscle is maintained with a higher pool of stem cells. The proportions of myogenic, adipogenic, and multipotent progenitors could also be significant in illustrating the activity of these stem cells. Prospective analyses of these cells, as well as satellite cells, could provide a more well-defined characterization of stem cell activity and interactions within skeletal muscle.

CT images have been analyzed to assign whole body values of muscle CSA, muscle radiation attenuation, and adipose tissue CSA to patients in several studies (2, 16, 27). Biopsies have also been gathered to understand mechanisms by which muscle regenerates (8). However, it is important to note that the information about cells from biopsies provide a view into a minute portion of the muscle. Previous studies have not

been conducted in the cancer realm to indicate how the structure of muscle is affected by cellular interactions. In order to create a comprehensive skeletal muscle profile, future analyses may also include additional stains to the ones presented such as esterase staining used to identify denervation of the fibres, as the presence of angular myofibres and pyknotic nuclei were noted and esterase staining will discern whether this is a neurogenic factor. Overall, it is essential to combine the cellular, structural, and whole-body segments of information in order to complete an illustration of an individual muscle. To date, this is the only study that has attempted to investigate all of these components from one patient. Fatty infiltration is a recurring theme in the discussion of muscle wasting, and if a profile is collected for each patient, we can determine the extent to which this phenomenon affects the cellular makeup, structure, and overall composition of muscle in cancer patients

Table 3-1: Current literature on morphological analyses of muscle from biopsies of cancer patients.

Reference (Reference number)	Muscle biopsied	Characteristics of Cancer Patients		Characteristics of Controls		Investigating	Major morphological findings (cancer patients in comparison to control)
		n	Diagnosis and/or Phenotype	n	Phenotype		
Weber et al., 2009 (10)	Vastus lateralis	10 male, 9 female	Gastrointestinal cancer; >10% weight loss	10 male, 9 female	Healthy; matched for age, sex, and height	Myofiber size	Lower BMI, MCSA, and total fibre size; quadricep muscle strength was the same when normalized to MCSA
Zampieri et al., 2010 (11)	Rectus abdominis	10 (sex not specified)	Newly diagnosed colorectal cancer; phenotype not specified	7 (sex not specified)	Non- neoplastic undergoing laparoscopic surgery	Morphometric analyses, ATPase histochemistry and immunohistochemical analysis of markers of muscle denervation and injury-induced muscle regeneration	Higher percentage of myofibers with central nuclei (as well as nuclei just internalized). (30% of patients, found small MHC- emb+ myofibers; 50%

							of patients, large N-CAM+ myofibres; none of either found in controls)
Stephens et al., 2011 (12)	Rectus abdominis	11 male, 8 female	Upper gastrointestinal cancer; weight losing	2 male, 4 female	Non-cancer: weight stable, undergoing elective abdominal surgery	Electron microscope investigation of intramyocellular lipid droplets	Increased lipid droplet number and size (in diameter); mean lipid number count correlated positively with weight loss severity
He et al., 2013 (8)	Rectus abdominis	11 male, 8 female	Pancreatic cancer; weight losing	3 male, 2 female, 1 not determined	Healthy, weight-stable undergoing minor surgical procedures	PAX7+ Satellite cell activity; Electron microscope investigation of muscle damage	Muscle exhibited membrane alterations and increased IgG staining not detected in control; overexpression of Pax7 in cancer patients

BMI: body mass index, MCSA: muscle cross-sectional area; MHC-emb: embryonic myosin heavy chain; N-CAM: neural cell

∞ adhesion molecule

Table 3-2: Cell isolation procedures.

Patient	Enzymatic Digestion (collagenase-dispase solution)	Wash	Centrifugation for adipocyte isolation	Centrifugation for mononuclear cell isolation	Resuspension of mononuclear cell pellet	Conditions	Redigestion of filtrate
2	Total of 710 μ L iced enzyme solution, incubated at 37°C for total of 20 min	Total of 710 μ L iced culture medium + 20% FBS	200 x g at 4°C for 5 min	800 x g at 4°C for 5 min	1 mL PBS	N/A	No
3			200 x g at 4°C for 10 min				
4							
5	Total of 4.5 mL iced enzyme solution with added calcium chloride , incubated at 37°C for total of 20 min	Total of 15 mL iced culture medium + 20% FBS	200 x g at 4°C for 10 min	800 x g at 4°C for 5 min	1 mL PBS + 143 μL of RBC lysis buffer	N/A	Yes
6							
7							
8							
10						No	
11	Yes						
12	37°C for total of 20 min	20% FBS				Different RBC lysis buffers conditions	Yes

13					1 mL PBS	Addition of different culture media; Addition of RBC lysis buffer	Yes
14						N/A	
15	Total of 4.5 mL enzyme solution with added calcium chloride (pre-warmed to 37°C), incubated at 37°C for total of 20 min	Total of 9 mL culture medium + 20% FBS, pre-warmed to room temperature	200 x g at 21°C for 10 min	800 x g at 21°C for 5 min	1 mL PBS + RBC lysis buffer	Adipocyte count in muscle vs. adipose tissue	No
16						Addition of RBC lysis buffer	
17					1 mL PBS		
19						N/A	Yes

The table indicates the changes made to the isolation protocol as described above. PBS = phosphate buffer saline, RBC = red blood cell.

Table 3-3: Antibody combinations used in flow cytometry analysis.

Well number	1	2	3	4	5	16
<i>Extracellular Antibodies</i>	Cells only	CD34/PE CD56/APC CD15/FITC	CD34/PE CD15/FITC	CD34/PE CD56/APC	CD15/FITC CD56/APC	Triple stain duplicate
Well number	6	7	8	9	10	17
<i>Intracellular Antibodies</i>	Cells only	PAX3/PE PAX7/FITC MyoD/AF594	PAX3/PE PAX7/FITC	PAX3/PE MyoD/AF594	PAX7/FITC/ MyoD/AF594	Triple stain duplicate
Well number	11	12	13	14	15	18
<i>Intracellular/ Extracellular Antibodies</i>	Cells only	PAX7/FITC CD34/PE CD56/APC	PAX7/FITC CD34/PE	PAX7/FITC CD56/APC	CD34/PE CD56/APC	Triple stain duplicate

These wells summarize the antigens for which antibodies are to be used in the flow cytometry for the identification of satellite cells and multipotent progenitors. Wells 1-5, 16 were labeled with antibodies against cell surface antigens only, wells 6-10, 17 against nuclear antigens only, and 11-15, 18 against both cell surface and nuclear antigens. CD: cluster of differentiation, PAX: Paired box protein, PE: phycoerythrin, FITC: fluorescein isothiocyanate, APC: allophycocyanin, AF594: Alexa Fluor 594.

Table 3-4: Cell counts per milliliter of cell suspension assessed under haemocytometer.

Pt	Conditions (if any)	Adipocyte layer after 200 x g centrifugation										Pellet after 800xg spin	Redigestion of filtrate (if available)	% of all cells found in filtrate	Issues identified								
		Layer number																					
		1	2	3	4	5	6	7	8	9	Total												
		Cell counts per mL, thousands																					
2	N/A	20	N/A							20	2,430	N/A	N/A	N/A									
3		60								60	4,590												
4		0								0	0												
5		20								20	20												
6		52								84	52			44	72	72	40	44	44	504	8,328		
7		16								16	12			12	20	0	0	4	8	88	8,480		
8		0								0	0			0	0	0	0	0	0	0	6,124		
10		0								4	0			12	0	0	4	0	0	20	1,072		
11		0								0	0			0	0	0	0	0	0	0	4,848	8	0.20%

Table 3-5: Skeletal muscle profile of male cancer patients with histological and immunofluorescent analyses.

Patient Number	14	27	26	23	24	28	22	Average of sampled patients (Mean ± SD)
Age	65	81	78	60	65	57	62	67 ± 8
CT-derived characteristics								
<i>Total Lumbar Muscle</i> CSA (cm ²)	109.0	130.4	141.5	170.4	175.7	206.0	213.8	163.8 ± 36.0
Mean muscle radiation attenuation (HU)	7.1	32.5	34.5	37.7	54.4	23.5	39.3	32.7 ± 14.6
Skeletal muscle index (cm ² /m ²)	36.4	53.4	46.7	49.5	55.5	67.3	68.2	53.9 ± 11.3
Intermuscular adipose (cm ²)	75.0	3.8	9.6	9.2	4.1	29.9	5.2	19.5 ± 26.1
Visceral adipose (cm ²)	376.1	28.6	196.3	52.2	199.8	317.4	181.9	193.2 ± 126.5
Subcutaneous adipose (cm ²)	479.0	52.0	178.2	61.2	232.9	329.4	255.9	226.9 ± 150.2
Total adipose (cm ²)	930.1	84.4	384.1	122.6	436.8	676.7	443.0	439.7 ± 296.2
<i>Rectus abdominus</i> CSA (cm ²)	11.0	11.2	11.2	12.0	15.7	18.9	18.7	14.1 ± 3.6
Mean muscle radiation attenuation (HU)	-5.7	40.9	16.0	24.8	37.3	13.8	34.3	23.1 ± 16.4
Intermuscular adipose (cm ²)	12.6	0.0	0.7	0.2	0.2	1.2	0.3	2.2 ± 4.6

Sarcopenic status*	1	0	1	1	0	0	0	--
Myosin heavy chain content (%)								
Not detectable								
IIX			22.6		21.9			22.3 ± 0.5
IIA	27.9	N/A	58.4	N/A	42.3		N/A	42.9 ± 15.3
I	72.1		19		35.8			42.3 ± 27.1
Embryonic	0		0		0			0.0 ± 0.0
Lipid analysis								
Total triglyceride fatty acids (mg/g)	25475.1		13203		4143.8			14274.0 ± 10705.9
Saturated Fatty Acids (%)	30		34.1		32.6			32.2 ± 2.1
Monounsaturated Fatty Acids (%)	56		51.1		50.9			52.7 ± 2.9
n-6 Fatty Acids (%)	12.5		12.4		14			13.0 ± 0.9
n-3 Fatty Acids (%)	1.3		1.2		2.2			1.6 ± 0.6
Morphological properties								
Myofibre CSA (mm ²) †	5758 ± 3117	5479 ± 2570	7016 ± 3485	5253 ± 1781	5026 ± 2156	4441 ± 1971	4873 ± 1495	5407 ± 827
Myofibre Diameter (mm) †	119 ±	107 ±	134 ±	111 ±	108 ±	95 ±	109 ±	112 ± 12

	37	28	± 40	25	24	23	20	
Intramyocellular lipids‡	++	++	++	+	++	+++	++	--
Intermuscular adipocytes‡	+++	+	+++	++	++	++	+	--

Stem cell analysis (Immunofluorescence; number per 100 myofibres)

Multipotent progenitors	0.52	0.69	1.84	1.19	2.24	1.69	1.1	1.3 ± 0.6
Myogenic Progenitors	1.4	1.62	0	0.48	2.24	1.27	0.88	1.1 ± 0.7
Adipogenic Progenitors	1.57	0.92	1.47	0.72	2.99	0.85	0.66	1.3 ± 0.8

Stem cell analysis (Flow cytometry; % of MNCs)

Multipotent progenitors	N/A	1.5	0.74	5.26	2.5 ± 2.4
Myogenic Progenitors		0.85	0.01	4.26	1.7 ± 2.3
Adipogenic Progenitors		0.1	0	0.33	0.1 ± 0.2
Quiescent Satellite Cells		4.12			--
Proliferating Myoblasts		0.1	N/A		--
Myocyte		0.08			--

Areas marked N/A indicate that the specified analysis was not done for the patient.

* 1 indicates sarcopenic, 0 indicates not sarcopenic. †Parameters measured as mean ± standard deviation of muscle fibres. ‡ Parameters analyzed to be mild (+), moderate (++), or severe (+++). CT: computed tomography, CSA: cross-sectional area.

Table 3-6: Extremes of phenotype: Direct comparison of skeletal muscle profile of male cancer patients P14 and P24.

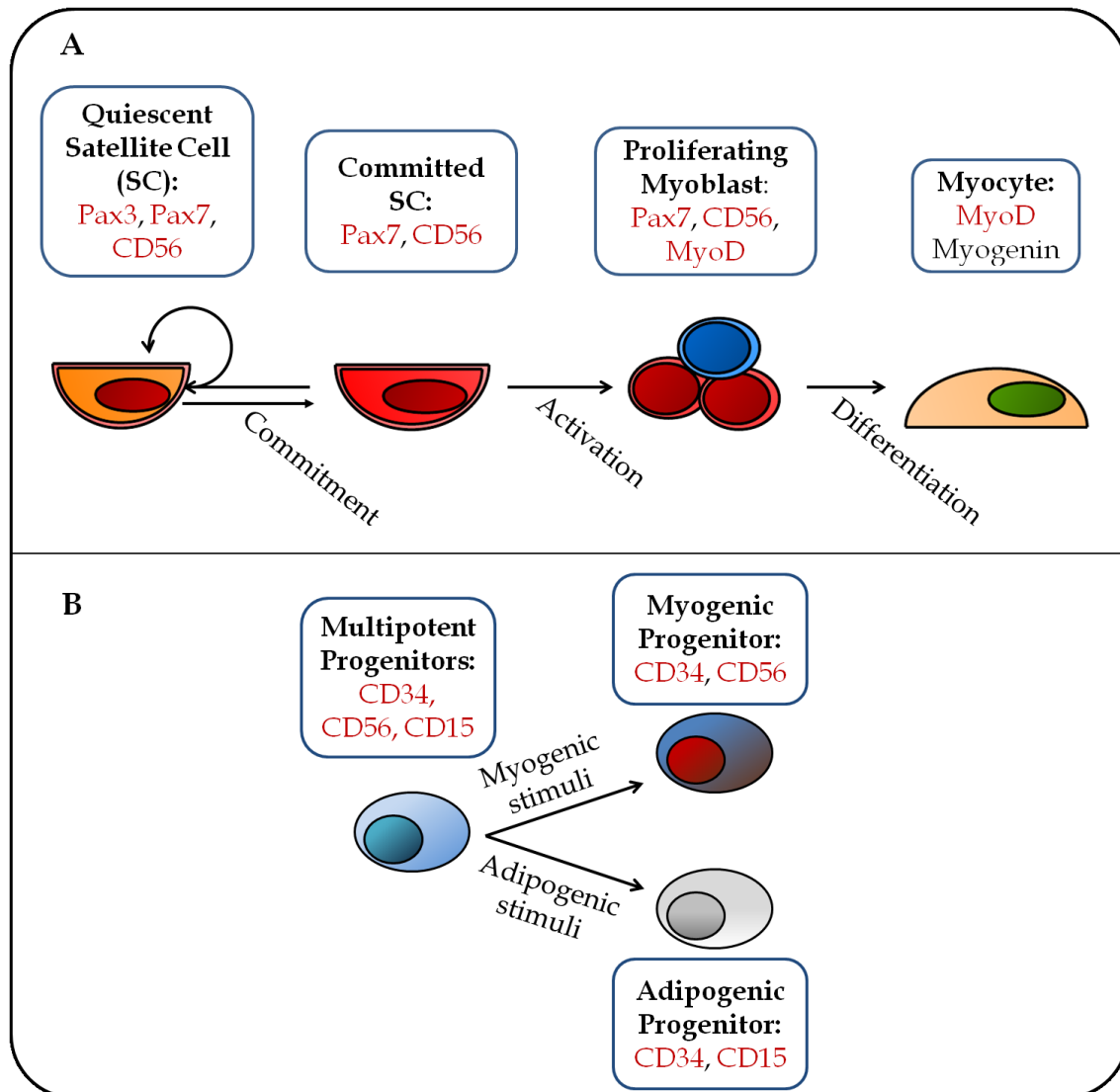
Patient Number	14	24
Age	65	65
CT-derived characteristics		
Muscle CSA (cm ²)	109.0	175.7
Mean muscle radiation attenuation(HU)	7.1	54.4
SMI (cm ² /m ²)	36.4	55.5
IMAT (cm ²)	75.0	4.1
VAT (cm ²)	376.1	199.8
SAT (cm ²)	479.0	232.9
TAT (cm ²)	930.1	436.8
Rectus abdominis muscle only - CSA (cm ²)	11.0	15.7
Mean muscle radiation attenuation (HU)	-5.7	37.3
RA only – IMAT (cm ²)	12.6	0.2
Sarcopenic status*	1	0
MHC content (%)		
IIX	0.0	21.9
IIA	27.9	42.3
I	72.1	35.8
Embryonic	0.0	0.0
Lipid content		
Total Triglycerides (µg/g)	25475.1	4143.8
Saturated Fatty Acids (%)	30.0	32.6
Monounsaturated Fatty Acids (%)	56.0	50.9
n-6 Fatty Acids (%)	12.5	14.0
n-3 Fatty Acids (%)	1.3	2.2
Morphological properties		
Myofibre CSA (µm ²) †	5758 ± 3117	5026 ± 2156
Myofibre Diameter (µm) †	119 ± 37	108 ± 24

Intramyocellular lipids ‡	++	++
Intermuscular adipocytes ‡	+++	++
Immunofluorescence stem cell analysis (number per 100 myofibres)		
Multipotent progenitors	0.52	2.24
Myogenic Progenitors	1.40	2.24
Adipogenic Progenitors	1.57	2.99

* 1 indicates sarcopenic, 0 indicates not sarcopenic. †Parameters measured as mean \pm standard deviation of muscle fibres. ‡ Parameters analyzed to be mild (+), moderate (++), or severe (+++). CT: computed tomography, CSA: cross-sectional area, SMI: skeletal muscle index, IMAT: intermuscular adipose tissue, VAT: visceral adipose tissue, SAT: subcutaneous adipose tissue, TAT: total adipose tissue, RA: rectus abdominis, MHC: myosin heavy chain, ND: not determined due to missing heights.

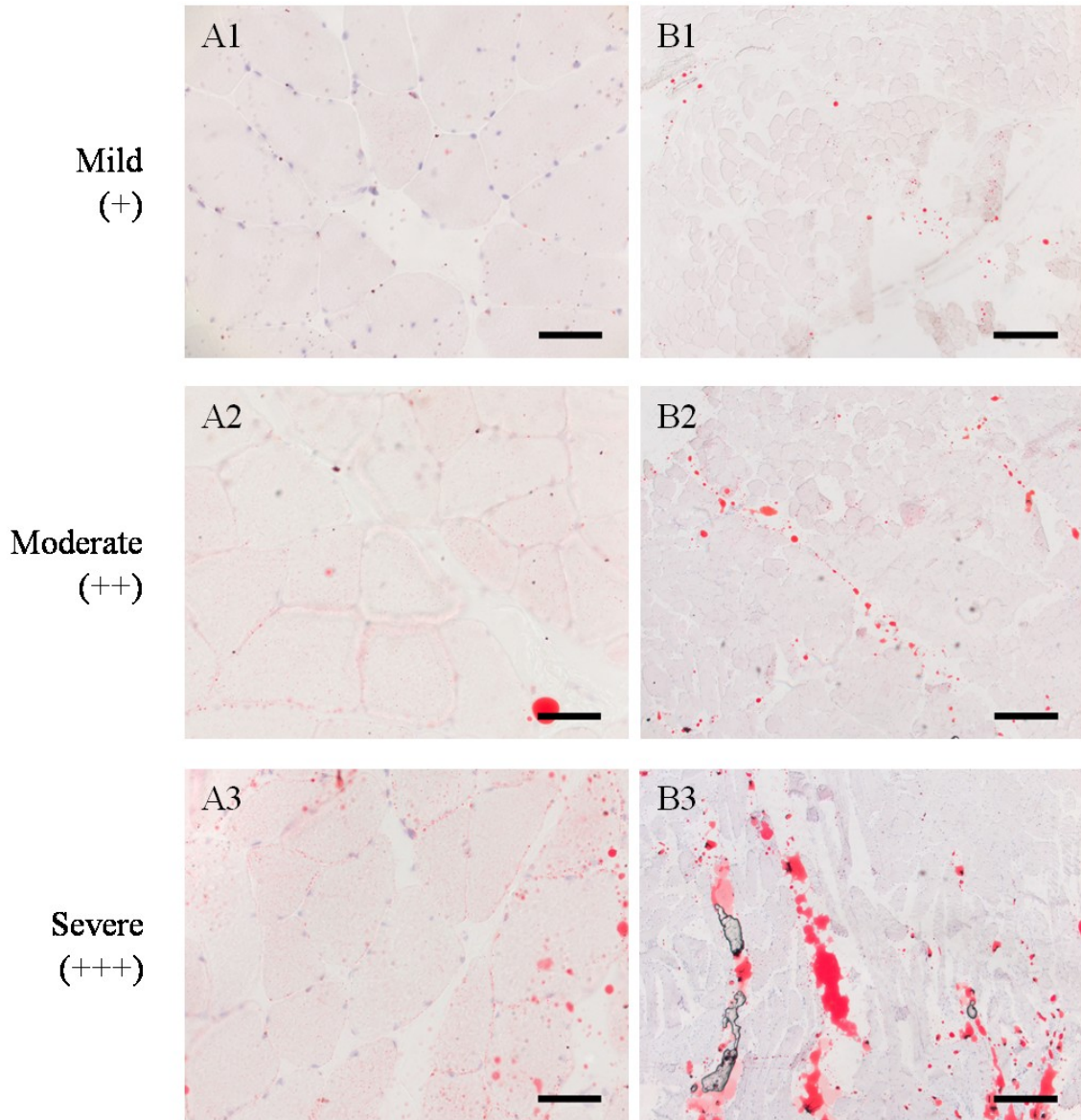
Figures

Figure 3-1: Satellite cell and multipotent progenitor life cycles.



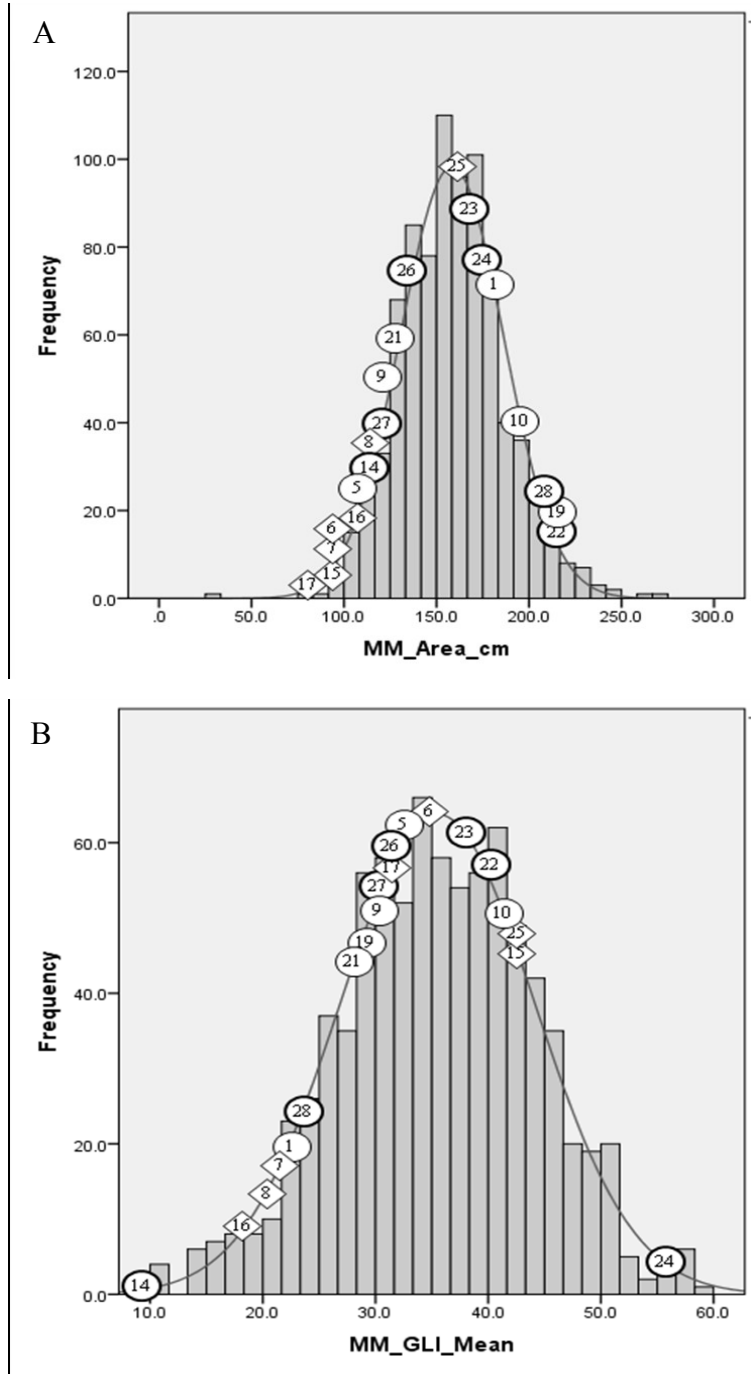
(A) Satellite cells may become committed to the myogenic program when the muscle receives a stimulus. The committed SC can then revert to its quiescent state or become activated. As a proliferating myoblast, the cell may differentiate to become a myocytes, whereupon it may fuse to pre-existing myofibres. (B) Multipotent progenitors may become myogenic or adipogenic upon receiving a stimulus. SC: satellite cells, CD: cluster of differentiation, PAX: paired box transcription factor.

Figure 3-2: Pathological classification of intermuscular adipose tissue and intramyocellular lipid droplets.



Fatty infiltration categorized as mild (+), moderate (++) or severe (+++) for intramyocellular lipid droplets (A; Scale bar 50 μ m) and intermuscular adipocytes (B; Scale bar 400 μ m). Each panel is a different patient and red areas depict lipids positively stained with Oil Red O.

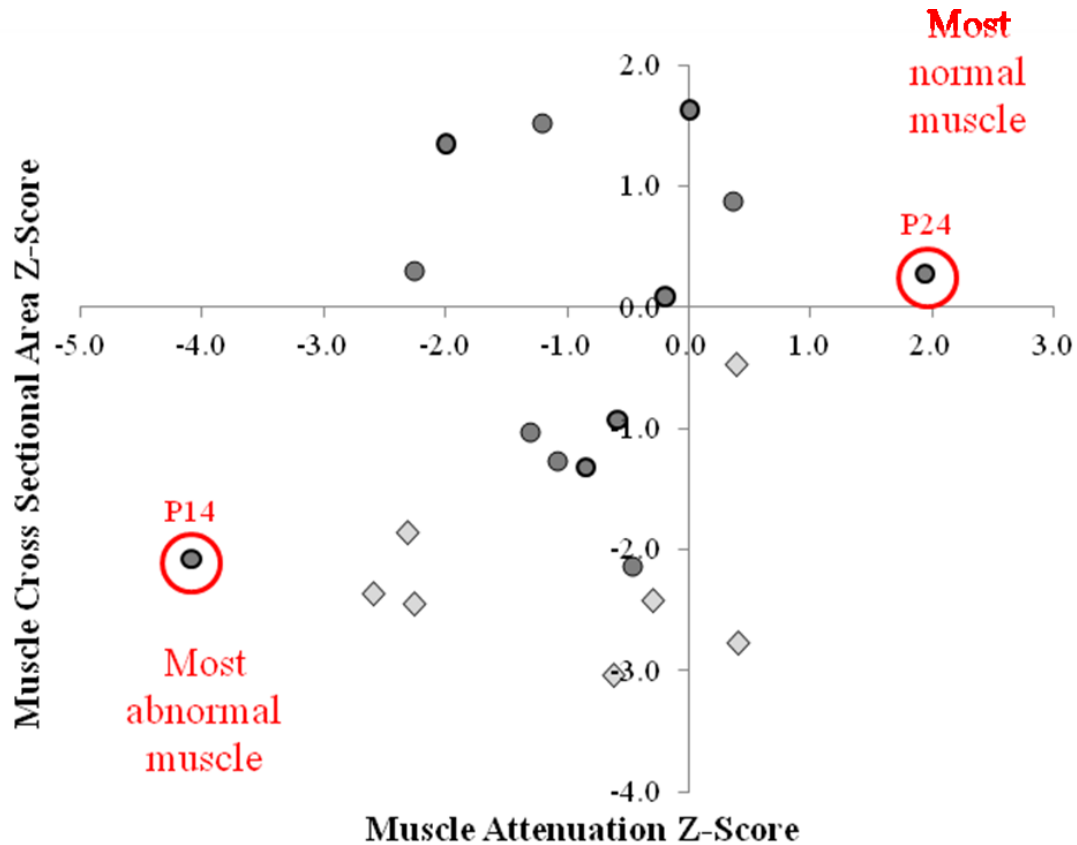
Figure 3-3: Muscle biopsy patients placed within larger cohort of lung and gastrointestinal cancer patients (n=828) for muscle cross-sectional area (A) and attenuation (B).



Larger cohorts of patients provided by Martin, 2013 (16) for muscle cross-sectional area (MM_Area_cm) and mean attenuation (MM_GLI_Mean). Patients represented with

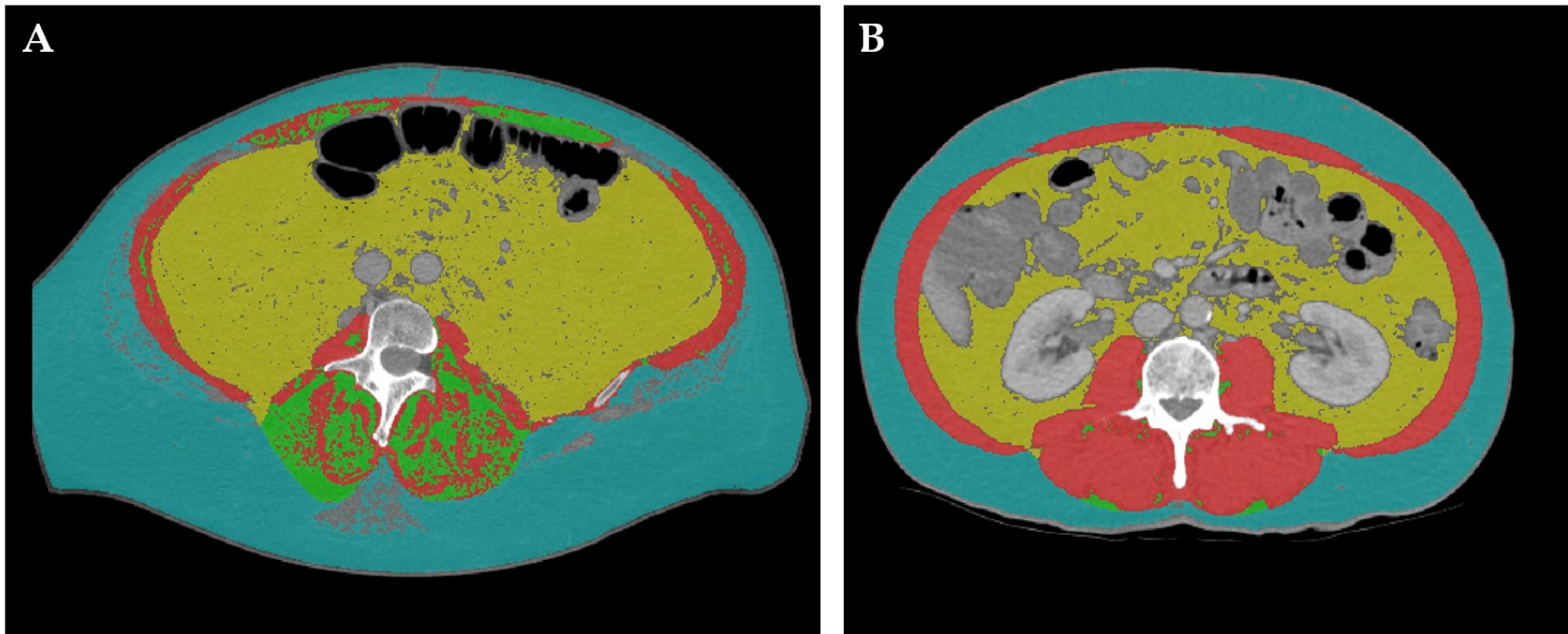
circle indicate males and those represented by diamonds indicate females. Points with bolded outline are patients included in the analysis of morphological features.

Figure 3-4: Z-scores of muscle cross-sectional area and attenuation for muscle biopsy patients within larger dataset of patients.



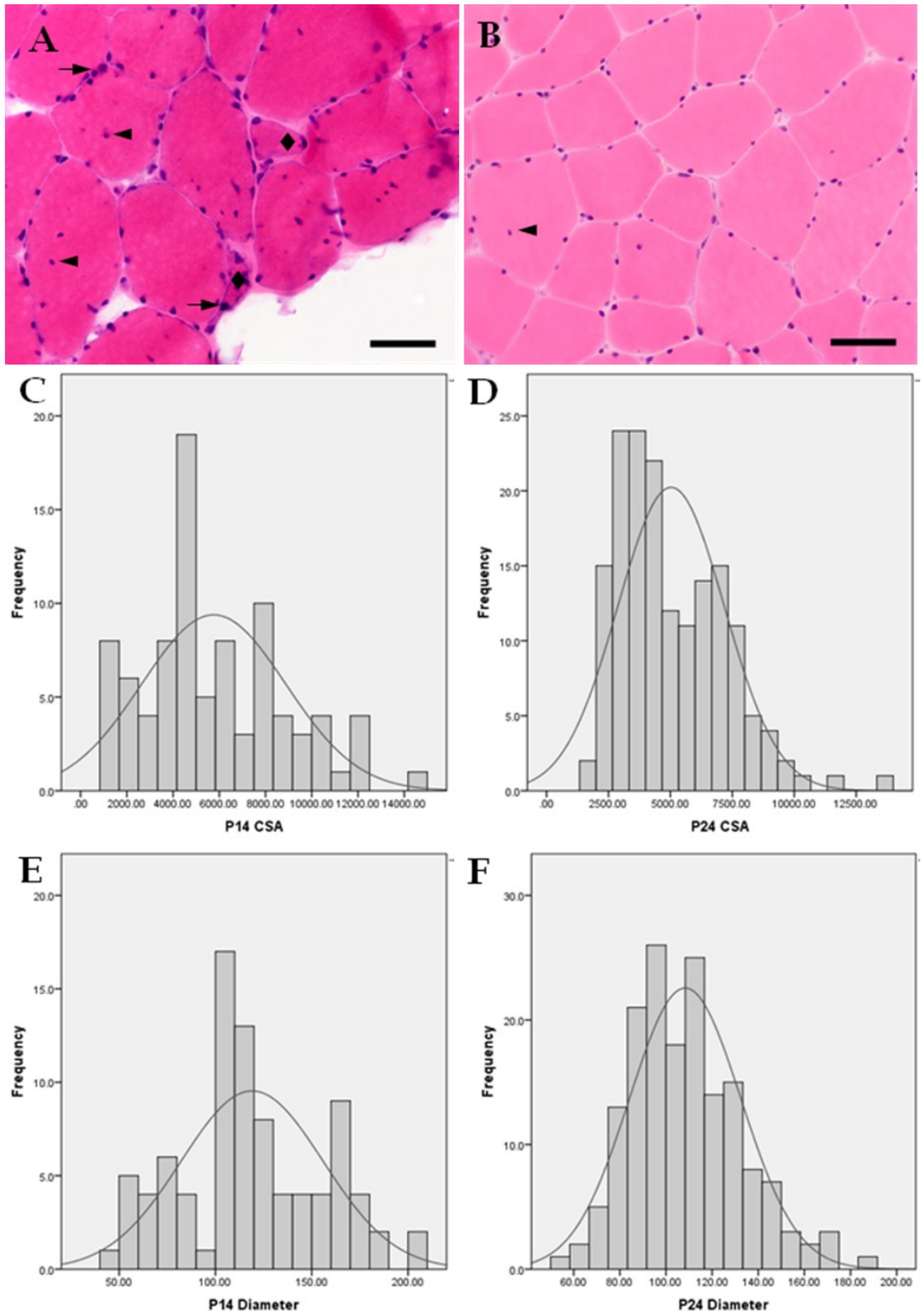
Z-scores of muscle cross-sectional area and attenuation; Z-scores are unitless. Upper right and lower left quadrants represent most normal and most abnormal muscle, respectively. Patients represented with circle indicate males and those represented by diamonds indicate females. Points with bolded outline are patients included in the analysis of morphological features, and patients P14 and P24 are circled.

Figure 3-5: Computed tomography images analyzed for patients P14 (A) and P24 (B).



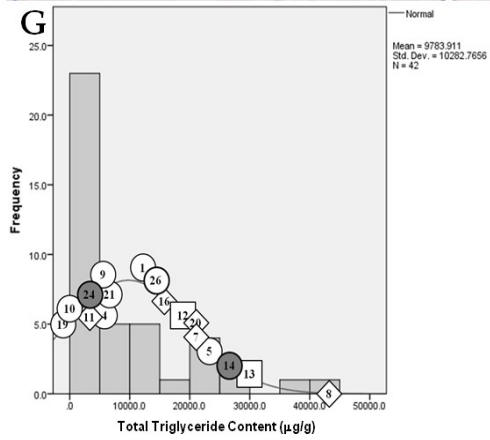
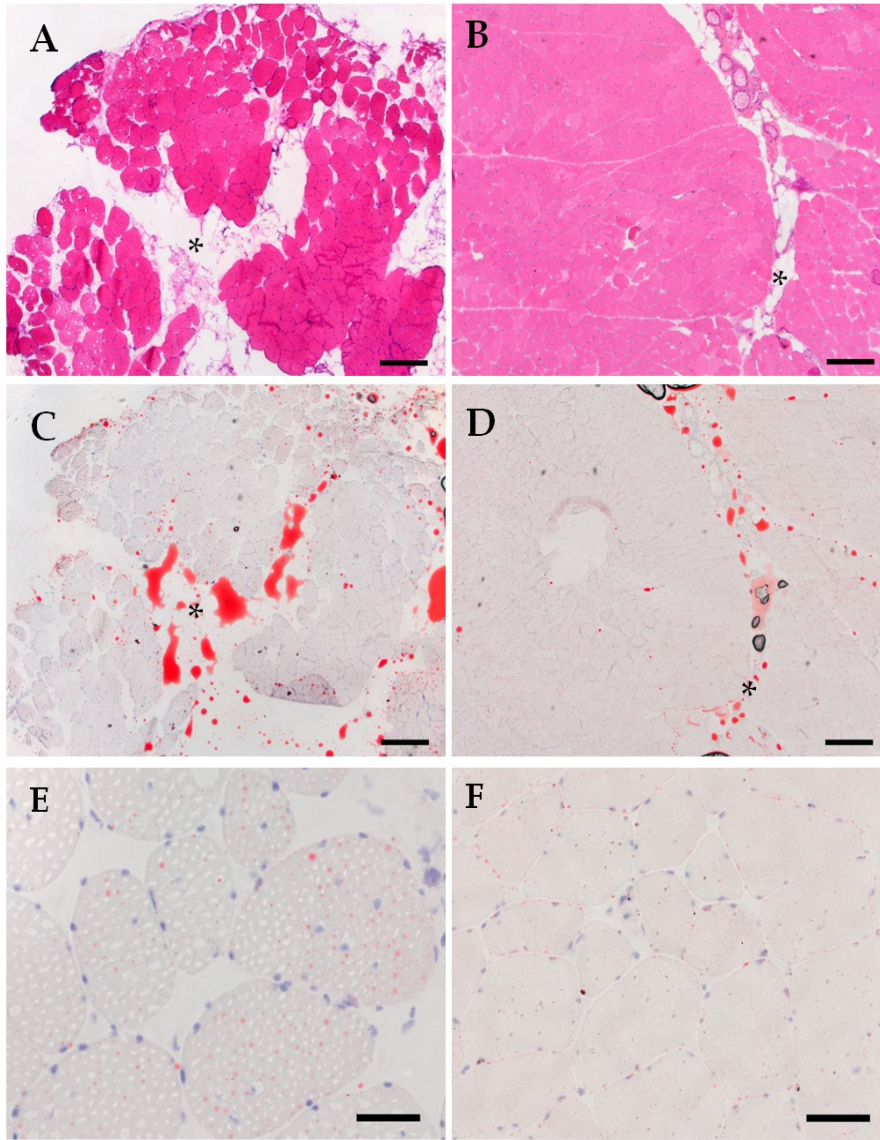
Computed tomography images at third lumbar vertebra analyzed for muscle (red), intermuscular adipose tissue (green), visceral adipose tissue (yellow), and subcutaneous adipose tissue (teal). Patient P14 (A) has low muscle cross-sectional area and attenuation, and patient P24 (B) has high muscle cross-sectional area and attenuation.

Figure 3-6: Haematoxylin and eosin staining of tissue sections from patients P14 and P24 allow measurements of myofibres and exhibit abnormalities in wasting.



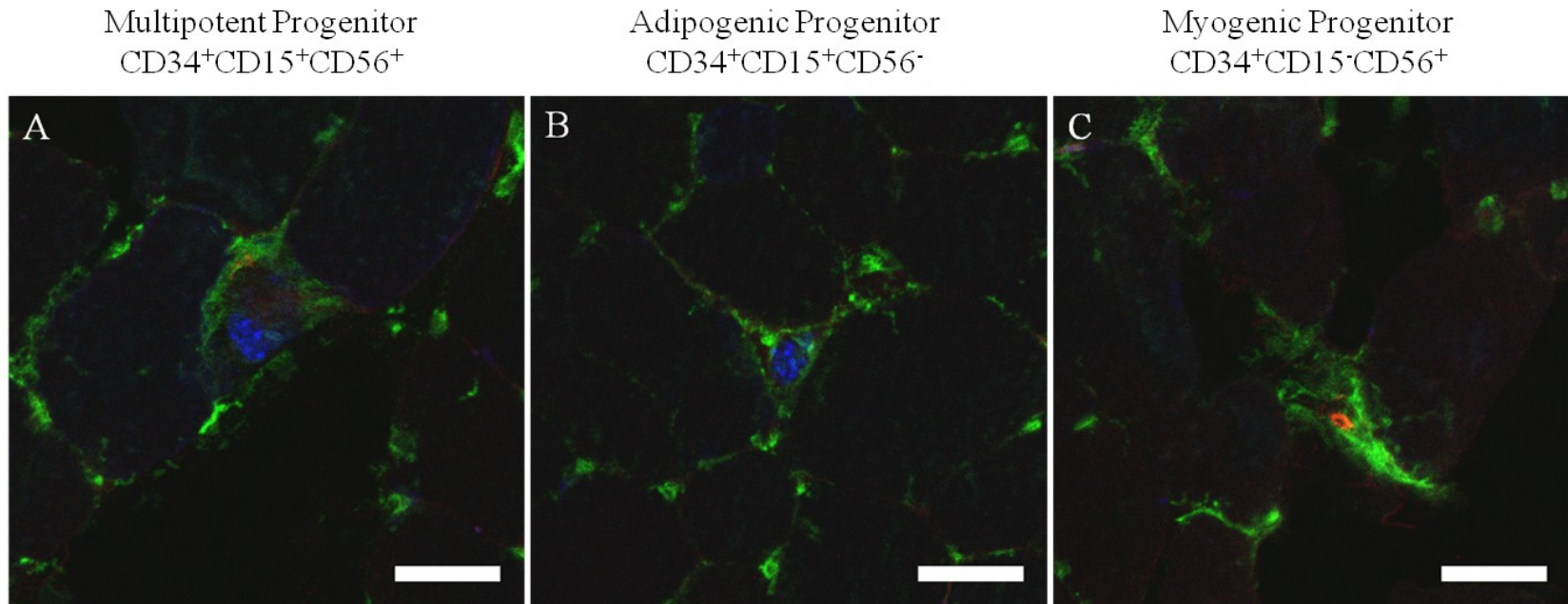
Myofibres represented by red-pink polygonal shapes and nuclei depicted as blue dots in haematoxylin and eosin stains for patients P14 (A) and P24 (B). Cross-sectional areas (CSA) and diameters are measured for patients P14 (C, E) and P24 (D, F). Arrows denote pyknotic nuclei, arrowheads denote centrally located nuclei, and ♦ mark myofibres that are angular in shape. Scale bars: 50 μm .

Figure 3-7: Haematoxylin and eosin and Oil Red O staining of tissue sections from patients P14 and P24 highlight areas of fat in and between muscle.



Myofibres represented by red-pink polygonal shapes and nuclei depicted as blue dots in haematoxylin stain (A, B). Positive staining for triglycerides is in red in Oil Red O stains (C-F). Patients with triglyceride measurements are placed along a distribution of triglyceride fatty acid data from rectus abdominis muscle biopsies from a larger set of lung, gastrointestinal cancer patients (n=42; unpublished data, Aubrey, Putman, Mazurak). Dark circles to the left and right of distribution represent patients P24 and P14, respectively (G). Asterisk (*) denotes infiltration of adipocytes. Scale bars for panels A-D: 300 μm ; scale bars for panels E, F: 50 μm .

Figure 3-8: Multipotent, adipogenic, and myogenic progenitors identified in interstitium of skeletal muscle.



Immunofluorescent staining for markers CD34 (green), CD15 (blue), and CD56 (red), to identify CD34⁺CD15⁺CD56⁺ multipotent (A), CD34⁺CD15⁺CD56⁻ adipogenic (B), and CD34⁺CD15⁻CD56⁺ myogenic progenitors (C). Scale bar: 50 μ m.

References

1. Mourtzakis M, Prado CM, Lieffers JR, et al. A practical and precise approach to quantification of body composition in cancer patients using computed tomography images acquired during routine care. *Appl Physiol Nutr Metab*. 2008;33(5):997–1006.
2. Prado CM, Sawyer MB, Ghosh S, et al. Central tenet of cancer cachexia therapy: do patients with advanced cancer have exploitable anabolic potential? *Am J Clin Nutr*. 2013;98(4):1012–1019.
3. Pallafacchina G, Blaauw B, Schiaffino S. Role of satellite cells in muscle growth and maintenance of muscle mass. *Nutr Metab Cardiovasc*. 2012;23(S1):S12-18.
4. Mitchell KJ, Pannérec A, Cadot B, et al. Identification and characterization of a non-satellite cell muscle resident progenitor during postnatal development. *Nat Cell Biol*. 2010;12(3):257–266.
5. Joe AWB, Yi L, Natarajan A, et al. Muscle injury activates resident fibro/adipogenic progenitors that facilitate myogenesis. *Nat Cell Biol*. 2010;12(2):153–163.
6. Pannérec A, Marazzi G, Sassoon D. Stem cells in the hood: the skeletal muscle niche. *Trends Mol Med*. 2012;18(10):599-606.

7. Pisani DF, Clement N, Loubat A, et al: Hierarchization of myogenic and adipogenic progenitors within human skeletal muscle. *Stem Cells* 28(12):2182–2194, 2010.
8. He WA, Berardi E, Cardillo VM, et al. NF-kappaB-mediated Pax7 dysregulation in the muscle microenvironment promotes cancer cachexia. *J Clin Invest.* 2013;123(11):4821.
9. Schiaffino S, Dyar KA, Ciciliot S, et al. Mechanisms regulating skeletal muscle growth and atrophy. *FEBS J.* 2013;280(17):4294-4314.
10. Weber M-A, Krakowski-Roosen H, Schröder L, et al. Morphology, metabolism, microcirculation, and strength of skeletal muscles in cancer-related cachexia. *Acta Oncol.* 2009;48(1):116-124.
11. Zampieri S, Doria A, Adami N, et al. Subclinical myopathy in patients affected with newly diagnosed colorectal cancer at clinical onset of disease: evidence from the skeletal muscle biopsies. *Neurolog Res.* 2010;32(1):20-25.
12. Stephens NA, Skipworth RJ, MacDonald AJ, et al. Intramyocellular lipid droplets increase with progression of cachexia in cancer patients. *J Cachexia Sarcopenia Muscle.* 2011;2(2):111-117.
13. Corbu A, Scaramozza A, Badiali-DeGiorgi L, et al. Satellite cell characterization from aging human muscle. *Neurolog Res.* 2010;32(1):63–72.

14. Mackey AL, Andersen LL, Frandsen U, et al. Strength training increases the size of the satellite cell pool in type I and II fibres of chronically painful trapezius muscle in females. *J Physiol*. 2011;589(22):5503–5515.
15. McKay BR, Toth KG, Tarnopolsky MA, Parise G. Satellite cell number and cell cycle kinetics in response to acute myotrauma in humans: immunohistochemistry versus flow cytometry. *J Physiol*. 2010;588(17):3307–3320.
16. Martin L, Birdsell L, MacDonald N, et al. Cancer Cachexia in the Age of Obesity: Skeletal Muscle Depletion Is a Powerful Prognostic Factor, Independent of Body Mass Index. *J Clin Oncol*. 2013;31(12):1539–1547.
17. Prado CM, Baracos VE, McCargar LJ, et al. Body composition as an independent determinant of 5-fluorouracil-based chemotherapy toxicity. *Clin Cancer Res*. 2007;13(11):3264–3268.
18. Fanin M, Nascimbeni A, Angelini C. Muscle atrophy in Limb Girdle Muscular Dystrophy 2A: a morphometric and molecular study. *Neuropathol Appl Neurobiol*. 2013;39(7):762-771.
19. Nasis I, Kortianou E, Clini E, et al. Effect of rehabilitative exercise training on peripheral muscle remodelling in patients with COPD: targeting beyond the lungs. *Curr Drug Targets*. 2013;14(2):262-273.
20. Arnardottir S, Borg K, Ansved T. Sporadic inclusion body myositis: morphology, regeneration, and cytoskeletal structure of muscle fibres. *J Neurol Neurosurg Psychiatry*. 2004;75(6):917-920.

21. Acharyya S, Butchbach ME, Sahenk Z, et al. Dystrophin glycoprotein complex dysfunction: a regulatory link between muscular dystrophy and cancer cachexia. *Cancer Cell*. 2005;8(5):421–32.
22. Esfandiari N, Ghosh S, Prado C, et al. Age, obesity, sarcopenia, and proximity to death explain reduced mean muscle attenuation in patients with advanced cancer. *J Frailty Aging*. 2014;3(1):3-8.
23. Haugaard SB, Mu H, Vaag A, et al. Intramyocellular triglyceride content in man, influence of sex, obesity and glycaemic control. *Eur J Endocrinol*. 2009;161(1):57-64.
24. Goodpaster BH, Kelley DE, Thaete FL, et al. Skeletal muscle attenuation determined by computed tomography is associated with skeletal muscle lipid content. *J Appl Physiol*. 2000;89(1):104-110.
25. Aubrey J, Esfandiari N, Baracos V, et al. Measurement of skeletal muscle radiation attenuation and basis of its biological variation. *Acta Physiol*. 2014;210(3):489-497.
26. Goodpaster BH, Krishnaswami S, Resnick H, et al. Association between regional adipose tissue distribution and both type 2 diabetes and impaired glucose tolerance in elderly men and women. *Diabetes Care*. 2003;26(2):372-379.
27. Antoun S, Lanoy E, Iacovelli R, et al. Skeletal muscle density predicts prognosis in

patients with metastatic renal cell carcinoma treated with targeted therapies. *Cancer*.
2013;119:3377-84.

CHAPTER 4: Final Discussion

4.1 Introduction

A muscle biopsy can enlighten investigators and clinicians about the characteristics of skeletal muscle in an individual. In cancer, this is a particularly powerful notion as many patients suffer from muscle wasting, which has a significant impact on patient wellbeing and quality of life. The purpose of this work was to link population-based studies of cancer patients and the use of muscle biopsies to understand the biology of skeletal muscle wasting. This begins to fill a significant gap where the overwhelming majority of findings on cancer associated muscle wasting come from experimental animals. Only a few studies with a small number of biopsies from poorly characterized patient populations exist to describe the human homologue. Results from Chapter 2 revealed that there are multiple independent predictors of lower MA in advanced cancer patients, including age, sex, days to death, and lower muscle and higher total adipose tissue cross-sectional areas. In Chapter 3, CT image assessments and several analyses were completed on muscle biopsies collected from cancer patients receiving surgery to create a skeletal muscle profile. In patients with lower muscle cross sectional area, infiltration of fat into the muscle appeared to be the connection in the cellular, structural, and tissue composition analyses.

These results provide a suggestion into the way that muscle wasting is investigated, providing a complete examination of skeletal muscle biopsies in cancer. This may lead to a better treatment of patients due to an accurate comprehension of how their muscle is altered over the cancer trajectory. The following discussion expands upon the approaches taken in analyzing muscle biopsies. This topic will be expanded upon in

the cancer setting as well as in the non-cancer setting focused on stem cell analysis. Lastly, differences in the exploration of stem cells in rodent and human models will be discussed, with suggestions for further research progressing towards expanding knowledge of human muscle stem cells.

4.2 Human muscle biopsies are taken too infrequently and sporadically in the cancer setting to provide an absolute conclusion for skeletal muscle wasting

The history of muscle biopsies from cancer patients began in 1991 with a study of protein metabolism in cachectic cancer patients (1). There has been considerable focus on investigating the ubiquitin proteasome pathway involved in protein degradation with subsequent studies involving muscle biopsies (2, 3), as well as some studies on signaling (4, 5) and gene expression (6, 7). Only recently have there been morphological analyses of skeletal muscle tissue of cancer patients (8, 9). A relatively new venture in this population has been the study of skeletal muscle stem cells (10). These varying topics of investigation, however, have not been fully incorporated together to provide a meaningful representation of wasting in cancer. In fact, only one group has attempted to verify muscle loss in a single cancer patient using magnetic resonance imaging (11). Others have used bioelectrical impedance analysis to quantify fat-free mass, of which skeletal muscle is only a part (5, 9), but did not use measure loss over time. The presence of cachexia has been defined using weight loss, and if specified, would be considered as >10% in the previous 6 months (9, 12). In recent years, the assessment of weight-related parameters alone has been regarded as insufficient to confirm muscle wasting in cancer patients, as any individual may be sarcopenic regardless of their body size (13).

The use of CT images has barely been deployed in studies where muscle biopsies were evaluated. Considering that most patients included in prior studies would have had such images, this represents an obvious deficit of two key pieces of information. This includes muscle mass (i.e. whether any given individual was very muscular, around the median muscularity, or sarcopenic), as well as the presence of muscle loss, no change or even gain over time. While this has not been considered in earlier studies, there are now large databases showing these parameters in cancer patient populations, and future research can deploy purposeful sampling. This would allow a more powerful comparison of patients matched for sex, age, and disease parameters, who specifically differ in muscle mass or loss characteristics. Only one group has previously incorporated the use of CT images (12) when evaluating a biopsy. Mean lipid droplet number was negatively associated with estimated measures of intermuscular and visceral fat, but was not significantly correlated with muscle mass. However, as the CT-derived characteristics were not significantly associated with weight loss, the skeletal muscle indexes calculated were not further investigated as a parameter to relate with their ultimate focus of intramyocellular lipid droplets. A comparison based on CT image analysis does indeed appear difficult for this study design, as the cancer patients were matched against a non-cancer control group. This highlights the drawback to this imaging technique, as non-cancer control groups cannot be unnecessarily exposed to the radiation emitted by the scanner, though this is not an issue with cancer patients who already receive diagnostic CT images. However, patients within the cancer group in this study may have been stratified by muscle mass, even as a preliminary exploration considering the small sample size. Assessments of sarcopenic vs. non-sarcopenic cancer patients have been used in the

past to determine clinical outcomes related to muscle loss using CT images (13-15). A comparison of patients based on muscle mass was presented in Chapter 3, and this has the potential to continue providing a rapid, low cost measurement of muscle mass in future studies of cancer patients who provide muscle biopsies.

Other information such as comorbidities may also be provided for the more in-depth assessment of skeletal muscle to complement the histological staining, immunofluorescence, and flow cytometry analyses presented in Chapter 3. It is important to include possible comorbidities that may have an effect on the characteristics of skeletal muscle, such as obesity and diabetes which have been associated with fat infiltration within muscle (15). Though obtaining multiple muscle biopsies over time is not necessarily feasible, to provide a better understanding of the change in muscle and adipose tissue, serial CT images may be obtained and analyzed to track the characteristics of muscle as a whole. Also, it has been the practice to obtain the heights of the patients to normalize their muscle CSA. Patient cohorts can then be dichotomized as non-sarcopenic and sarcopenic, which has been previously correlated with decreased survival (16) and toxicity due to chemotherapy (17). However, if necessary, the CSA of muscle measured by CT imaging can provide some information about the muscle of a cancer patient in the context of a larger population, as was done in Chapter 3, and allow the analysis of muscle as a continuous variable, as was provided in Chapters 2.

4.3 Stem cell and fatty infiltration properties of muscle in rodent models are not well characterized or may not necessarily translate to humans

With the collection of administrative, CT image, and laboratory-based data included in Chapters 2 and 3, it can be concluded that there are multiple factors affecting

muscle and indicate that the complexity observed in humans exceed those emulated in experimental animal models. The observation of fatty infiltration in muscles of cancer patients was first reported to be of prognostic significance in 2011 (18) with supporting evidence to follow this claim (16, 19, 20). Specific genes relating to the synthesis of fat are seen to be expressed in muscle wasting in rodent models. Lipin 1, a gene encoding for a lipin protein involved in triglyceride synthesis, was upregulated in all forms of muscle wasting evaluated by Lecker et al. (21), including starvation, cancer, chronic renal failure, and diabetes. Similarly, perilipin 4, a gene encoding for a perilipin protein that coats lipid droplets, was expressed early in muscle atrophy induced by inflammation (22). However, fatty infiltration has not been reported in animal models of cachexia and this may be because of the young age of rats or mice in most studies.

As was revealed in Chapter 3, the presence of fat was detected using multiple means, including IMAT and mean muscle radiation attenuation derived from CT image analysis, morphological examinations through haematoxylin and eosin and Oil Red O staining, triglyceride content analysis, and the isolation of adipocytes through the cell separation procedure. From CT images, muscle CSA and attenuation present as sources of variation between patients. By extrapolating to a larger data set of gastrointestinal and lung cancer patients as was done in Chapter 3, the high variation in both of these properties was seen. The properties of muscle at two different conditions, wasting or healthier muscle, were observed in two patients at the extremes of both distributions. Particularly based upon the histological stains and the isolations of adipocytes (**Table 3-3**), there seem to be more adipocytes in wasting than normal muscle. The observances of low muscle CSA and attenuation suggests at the least in a portion of patients, there is

some mechanism working towards atrophy or loss of the myofibres or preventing regeneration, perhaps through the inhibition of stem cell activity. The presence of adipocytes implies that adipogenic progenitors are within the muscle to generate these fat cells.

Stem cells within skeletal muscle have also not been investigated to the same extent in humans as they have been in animal models. With the advent of flow cytometry techniques, attempts to isolate stem cells, particularly satellite cells have been made. The majority of studies regarding skeletal muscle stem cells have mostly been in the mouse (and some rat) models, whereas fewer investigations have been done on human muscle biopsies. Techniques for the isolation of satellite cells have varied between groups, but many continue to use pre-plating methods in both human (23, 24) and animal studies (25, 26). For the purposes of analyzing satellite cells at particular phases of quiescence and into the myogenic program, pre-plating would not be a suitable method, as satellite cells would activate following this isolation and lose their quiescence (27). Furthermore, many investigations are invested in quantifying satellite cells altogether, and use one biomarker to do so. In the development of satellite cell analysis in Chapter 3, this was avoided in order to obtain a full view of the satellite cell program, a concept that has been explored only to a limited extent in humans (28, 29). Despite these drawbacks, the quantification of total satellite cells overall appears to be similar between mouse and human models (<5% [30] and 2-4% [30, 31], respectively). However, there are differences in the characteristics that allow satellite cells to be identified and regulate their myogenic process. First, the biomarkers used to isolate satellite cells using flow cytometry and immunofluorescence is not completely identical. Though both can be detected with the

Pax7 marker, a suitable marker for mice (32), all satellite cells in humans are not identified by this marker (28), and require the CD56 marker present as well, a molecule not found in mice. Also until recently, CD34 was a marker being used to identify satellite cells (24) until it was confirmed by immunohistochemistry that CD34+ cells were not found in the satellite cell position (33).

A recent study comparing mouse and human satellite cells provided support for the idea that significant differences exist between these species (34). Human Pax7+ cells remained detectable in cell culture for a longer amount of time than the mouse Pax7+ cells, and also did not express the myogenic differentiation marker MyoD for a longer amount of time. This displacement in the timelines is reflected in gene expression data that MyoD expression increasing earlier in humans, but the expression of both MyoD and myogenin in mice occurs more quickly. This could be significant in that mouse satellite cells could be more inclined to enter the differentiation program. In addition, by knocking down particular markers on the cells in culture, they found that the absence of Pax7 does not result in reduced expression of Myf5 (another marker expected in the activated/proliferative phases of the satellite cells program), a result not repeated in the mouse cells. Lastly, they tested the responses of the cells to inflammatory cytokine IL1 β , a cytokine associated with muscle wasting (35). Surprisingly, this cytokine positively affected the growth of the stem cells in mice, but inhibited their activity in humans. This is also significant in the comparison between mouse and humans, particularly in cancer cachexia, due to the large role inflammation plays in this phenomenon. From this study, it appears that the timeline of the myogenic program, specific regulatory responses, and reaction to a particular pro-inflammatory cytokine are not shared by mouse and human

satellite cells. In addition to other differences between these populations, it would be significant to directly compare the two different satellite cells with a more robust method, such as flow cytometry.

In addition to satellite cells, there are a variety of other stem cells that have been identified and are currently under study. However, some have been identified and only studied in mice, such as FAPs (36, 37) and PICs (38), and other that have only been identified and subsequently isolated in human muscle (39). In these cases, it is not known whether these cells actually do exist in all species, and if so, how closely they resemble one another in activity and proportion of all mononuclear cells collected per muscle biopsy. The assessment of the presence and interactions of all known stem cells within skeletal muscle is a vast area that may be explored in the future. The incorporation of the knowledge regarding radiological characteristics, structural properties, and the sheer variety of stem cells will be fundamental in the future assessment and treatment of muscle wasting in cancer patients.

References

1. Shaw JH, Humberstone DA, Douglas RG, et al. Leucine kinetics in patients with benign disease, non-weight-losing cancer, and cancer cachexia: studies at the whole-body and tissue level and the response to nutritional support. *Surgery*. 1991;109(1):37-50.
2. Williams A, Sun X, Fischer JE, et al. The expression of genes in the ubiquitin-proteasome pathway is increased in skeletal muscle from patients with cancer. *Surgery*. 1999; 126(4):744-749.
3. DeJong CH, Busquets S, Moses AG, et al. Systemic inflammation correlates with increased expression of skeletal muscle ubiquitin but not uncoupling proteins in cancer cachexia. *Oncol Rep*. 2005; 14(1): 257-263.
4. Aversa Z, Bonetto A, Penna F, et al. Changes in myostatin signaling in non-weight-losing cancer patients. *Ann Surg Oncol*. 2012;19(4):1350-1356.
5. Busquets S, Deans C, Figueras M, et al. Apoptosis is present in skeletal muscle of cachectic gastro-intestinal cancer patients. *Clin Nutr*. 2007;26(5):614-618.
6. Pessina P, Conti V, Pacelli F, et al. Skeletal muscle of gastric cancer patients expresses genes involved in muscle regeneration. *Oncol Rep*. 2010;24(3):741-745.
7. Stephens NA, Gallagher IJ, Rooyackers O, et al. Using transcriptomics to identify and validate novel biomarkers of human skeletal muscle cancer cachexia. *Genome Med*. 2010;2(1):1-12.
8. Zampieri S, Doria A, Adami N, et al. Subclinical myopathy in patients affected with newly diagnosed colorectal cancer at clinical onset of disease: evidence from skeletal muscle biopsies. *Neurolog Res*. 2010; 32(1): 20-25.

9. Weber M-A, Krakowski-Roosen H, Schröder L, et al. Morphology, metabolism, microcirculation, and strength of skeletal muscles in cancer-related cachexia. *Acta Oncol.* 2009;48(1):116-124.
10. He WA, Berardi E, Cardillo VM, et al. NF-kappaB-mediated Pax7 dysregulation in the muscle microenvironment promotes cancer cachexia. *J Clin Invest.* 2013;123(11):4821.
11. Banduseela V, Ochala J, Lamberg K, et al. Muscle paralysis and myosin loss in a patient with cancer cachexia. *Acta Myol.* 2007;26(3):136.
12. Stephens NA, Skipworth RJ, MacDonald AJ, et al. Intramyocellular lipid droplets increase with progression of cachexia in cancer patients. *J Cachexia Sarcopenia Muscle.* 2011;2(2):111-117.
13. Prado CM, Lieffers JR, McCargar LJ, et al. Prevalence and clinical implications of sarcopenic obesity in patients with solid tumours of the respiratory and gastrointestinal tracts: a population-based study. *Lancet Oncol.* 2008; 9:629-635.
14. Prado CM, Sawyer MB, Ghosh S, et al. Central tenet of cancer cachexia therapy: do patients with advanced cancer have exploitable anabolic potential? *Am J Clin Nutr.* 2013;98(4):1012–1019.
15. Goodpaster BH, Thaete FL, Kelley DE. Thigh adipose tissue distribution is associated with insulin resistance in obesity and in type 2 diabetes mellitus. *Am J Clin Nutr.* 2000; 71(4): 885-855592.
16. Martin L, Birdsell L, MacDonald N, et al. Cancer Cachexia in the Age of Obesity: Skeletal Muscle Depletion Is a Powerful Prognostic Factor, Independent of Body Mass Index. *J Clin Oncol.* 2013;31(12):1539–1547.

17. Prado CM, Baracos VE, McCargar LJ, et al. Body composition as an independent determinant of 5-fluorouracil-based chemotherapy toxicity. *Clin Cancer Res*. 2007;13(11):3264–3268.
18. Sabel MS, Lee J, Englesbe MJ, et al. Sarcopenia as a prognostic factor among patients with stage III melanoma. *Ann Surg Oncol*. 2011;18(13):3579–3585.
19. Antoun S, Lanoy E, Iacovelli R, et al. Skeletal muscle density predicts prognosis in patients with metastatic renal cell carcinoma treated with targeted therapies. *Cancer*. 2013;119(18):3377-3384.
20. Esfandiari N, Ghosh S, Prado C, et al. Age, obesity, sarcopenia, and proximity to death explain reduced mean muscle attenuation in patients with advanced cancer. *J Frailty Aging*. 2014;3(1):3-8.
21. Braun TP, Zhu X, Szumowski, et al. Central nervous system inflammation induces muscle atrophy via activation of the hypothalamic--pituitary--adrenal axis. *J Exp Med*. 2011;208(12):2449-2463.
22. Lecker SH, Jagoe RT, Gilbert A, et al. Multiple types of skeletal muscle atrophy involve a common program of changes in gene expression. *FASEB J*. 2004;18:39-51.
23. Blau HM, Webster C. Isolation and characterization of human muscle cells. *Proc Natl Acad Sci*. 1981;78(9):5623-5627.
24. Lu SH, Wei CF, Yang AH, et al. Isolation and characterization of human muscle-derived cells. *Urology*. 2009;74(2):440-445.
25. Danoviz ME, Yablonka-Reuveni Z. Skeletal muscle satellite cells: background and methods for isolation and analysis in a primary culture system. *Methods Mol Biol*. 2012;798:21-52.

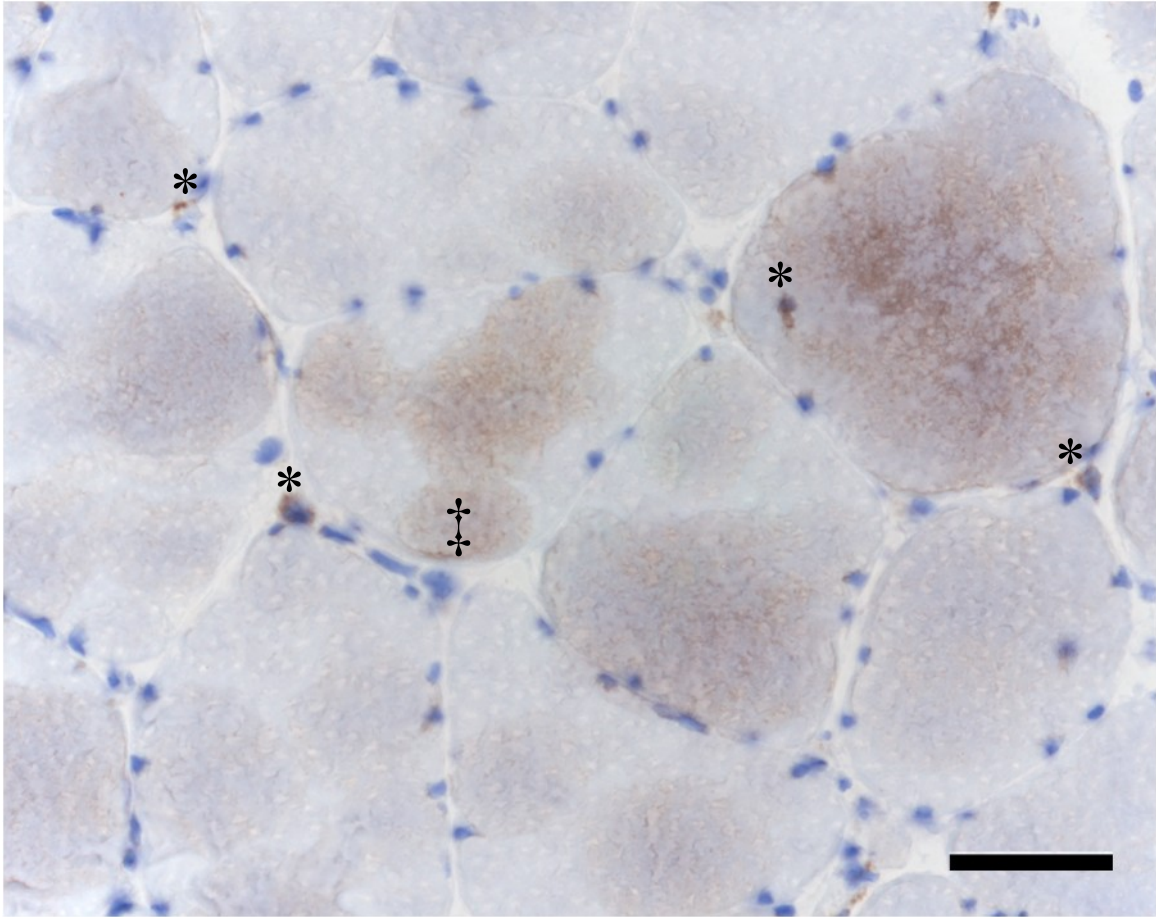
26. Schwarzkopf M, Coletti D, Sassoon D, et al. Muscle cachexia is regulated by a p53-PW1/Peg3-dependent pathway. *Genes Dev.* 2006;20(24):3440-3452.
27. Montarras D, Morgan J, Collins C, et al. Direct isolation of satellite cells for skeletal muscle regeneration. *Science.* 2005;309(5743):2064-2067.
28. Lindström M, Thornell LE. New multiple labelling method for improved satellite cell identification in human muscle: application to a cohort of power-lifters and sedentary men. *Histochem Cell Biol.* 2009;132(2):141-157.
29. Corbu A, Scaramozza A, Badiali-DeGiorgi L, et al. Satellite cell characterization from aging human muscle. *Neurol Res.* 2010;32(1):63-72.
30. Allbrook D, Han M, Hellmuth A. Population of muscle satellite cells in relation to age and mitotic activity. *Pathology.* 1971;3(3):233-243.
31. Schmalbruch H, Hellhammer U. The number of satellite cells in normal human muscle. *Anat Rec.* 1976;185(3):279-287.
32. Asakura A, Seale P, Girgis-Gabardo A, et al. Myogenic specification of side population cells in skeletal muscle. *J Cell Biol.* 2002;159(1):123-134.
33. Pisani DF, Dechesne CA, Sacconi S, et al. Isolation of a Highly Myogenic CD34-Negative Subset of Human Skeletal Muscle Cells Free of Adipogenic Potential. *Stem Cells.* 2010;28(4):753-764.
34. Bareja A, Holt JA, Luo G, et al. Human and Mouse Skeletal Muscle Stem Cells: Convergent and Divergent Mechanisms of Myogenesis. *PLoS One.* 2014;9(2):e90398.
35. Fearon KC, Glass DJ, Guttridge DC. Cancer cachexia: mediators, signaling, and metabolic pathways. *Cell Metab.* 2012;16(2):153-166.

36. Joe AWB, Yi L, Natarajan A, et al. Muscle injury activates resident fibro/adipogenic progenitors that facilitate myogenesis. *Nat Cell Biol.* 2010;12(2):153-163.
37. Mozzetta C, Consalvi S, Saccone V, et al. Fibroadipogenic progenitors mediate the ability of HDAC inhibitors to promote regeneration in dystrophic muscles of young, but not old Mdx mice. *EMBO Mol Med.* 2013;5(4):626-639.
38. Mitchell KJ, Pannérec A, Cadot B, et al. Identification and characterization of a non-satellite cell muscle resident progenitor during postnatal development. *Nat Cell Biol.* 2010;12(3):257-266.
39. Pisani DF, Clement N, Loubat A, et al. Hierarchization of myogenic and adipogenic progenitors within human skeletal muscle. *Stem Cells.* 2010;28(12):2182-2194.

Appendix A1

Immunohistochemistry: To observe the potential involvement of inflammatory cells, the markers CD3, CD8, and CD68 were used to identify T lymphocytes, specifically cytotoxic T lymphocytes, and macrophages, respectively. Frozen sections were fixed overnight in 10% formalin, and then blocked with FLEX peroxidase block (Dako SM801). The primary antibodies CD3, CD8, or CD68 were then applied with an incubation time of 20 minutes. FLEX+ Mouse (Dako, K8021) and FLEX+ Rabbit (Dako, K8009) secondary reagents were added for 15 minutes to the sections with CD68 and CD3, respectively, to amplify the signals of the primary antibodies. The FLEX/HRP labeled polymer was then added (Dako, SM802) for 30 minutes before adding the FLEX DAB+ Substrate-Chromogen (Dako, DM827). The slides were counterstained with hematoxylin for 5 minutes. At least one wash was done between each step. The slides were then rinsed with deionized water and kept at room temperature until analyzed. Slides were analyzed using a light microscope for areas of positive staining, shown as a brown stain due to horse radish peroxidase.

Figure A1. Infiltration of myofibres with CD68+ inflammatory cells.



Myofibres (blue) are infiltrated by cells positive for CD68 (monocytes and macrophages) Brown areas indicate positive staining (‡) and many have a distinct outline. Asterisk (*) denotes CD68+ cells surrounding nuclei both within and external to the myofibre. Scale bar: 50 μ m.

Bibliography

Acharyya S, Butchbach ME, Sahenk Z, et al. Dystrophin glycoprotein complex dysfunction: a regulatory link between muscular dystrophy and cancer cachexia. *Cancer Cell*. 2005;8(5):421–32.

Allbrook D, Han M, Hellmuth A. Population of muscle satellite cells in relation to age and mitotic activity. *Pathology*. 1971;3(3):233-243.

Arnardottir S, Borg K, Ansved T. Sporadic inclusion body myositis: morphology, regeneration, and cytoskeletal structure of muscle fibres. *J Neurol Neurosurg Psychiatry*. 2004;75(6):917-920.

Anderson DE, D'Agostino JM, Bruno AG, et al. Variations of CT-based trunk muscle attenuation by age, sex, and specific muscle. *J Gerontol A-Biol Sci Med Sci* 2013; 68:317-323.

Antoun S, Baracos V, Birdsall L, et al. Low body mass index and sarcopenia associated with dose-limiting toxicity of sorafenib in patients with renal cell carcinoma. *Ann Oncol*. 2010;21(8):1594–1598.

Antoun S, Lanoy E, Iacovelli R, et al. Skeletal muscle density predicts prognosis in patients with metastatic renal cell carcinoma treated with targeted therapies. *Cancer*. 2013;119(18):3377-3384.

Asakura A, Seale P, Girgis-Gabardo A, et al. Myogenic specification of side population cells in skeletal muscle. *J Cell Biol*. 2002;159(1):123-134.

Aubrey J, Esfandiari N, Baracos V, et al. Measurement of skeletal muscle radiation attenuation and basis of its biological variation. *Acta Physiol*. 2014;210(3):489-497.

Aversa Z, Bonetto A, Penna F, et al. Changes in myostatin signaling in non-weight-losing cancer patients. *Ann Surg Oncol*. 2012;19(4):1350-1356.

Bachmann J, Heiligensetzer M, Krakowski-Roosen H, et al. Cachexia worsens prognosis in patients with resectable pancreatic cancer. *J Gastr Surg*. 2008;12(7):1193–1201.

Banduseela V, Ochala J, Lamberg K, et al. Muscle paralysis and myosin loss in a patient with cancer cachexia. *Acta Myol*. 2007;26(3):136.

Baracos VE, Reiman T, Mourtzakis M, et al. Body composition in patients with non-small cell lung cancer: a contemporary view of cancer cachexia with the use of computed tomography image analysis. *Am J Clin Nutr* 2010; 91(4):1133S–1137S.

Bareja A, Holt JA, Luo G, et al. Human and Mouse Skeletal Muscle Stem Cells: Convergent and Divergent Mechanisms of Myogenesis. *PLoS One*. 2014;9(2):e90398.

Baumgartner RN, Koehler KM, Gallagher D, et al. Epidemiology of sarcopenia among the elderly in New Mexico. *Am J Epidemiol*. 1998;147(8):755–763.

Birbrair A, Zhang T, Wang Z-M, et al. Role of pericytes in skeletal muscle regeneration and fat accumulation. *Stem Cells Dev*. 2013;22(16):2298–2314.

Blau HM, Webster C. Isolation and characterization of human muscle cells. *Proc Natl Acad Sci*. 1981;78(9):5623-5627.

Braun TP, Zhu X, Szumowski, et al. Central nervous system inflammation induces muscle atrophy via activation of the hypothalamic--pituitary--adrenal axis. *J Exp Med*. 2011;208(12):2449-2463.

Busquets S, Deans C, Figueras M, et al. Apoptosis is present in skeletal muscle of cachectic gastro-intestinal cancer patients. *Clin Nutr*. 2007;26(5):614-618.

Cappellari O, Cossu G. Pericytes in Development and Pathology of Skeletal Muscle. *Circ Res*. 2013;113(3):341–347.

Carlson ME, Conboy IM. Loss of stem cell regenerative capacity within aged niches. *Aging Cell*. 2007;6(3):371–382.

Carlson ME, Suetta C, Conboy MJ, et al. Molecular aging and rejuvenation of human muscle stem cells. *EMBO Mol Med*. 2009;1(8-9):381–391.

Collins CA, Olsen I, Zammit PS, et al. Stem cell function, self-renewal, and behavioral heterogeneity of cells from the adult muscle satellite cell niche. *Cell*. 2005;122(2):289–301.

Corbu A, Scaramozza A, Badiali-DeGiorgi L, et al. Satellite cell characterization from aging human muscle. *Neurolog Res*. 2010;32(1):63–72.

Cosquéric G, Sebag A, Ducolombier C, et al. Sarcopenia is predictive of nosocomial infection in care of the elderly. *Briy J Nutr*. 2006;96(5):895–901.

Danoviz ME, Yablonka-Reuveni Z. Skeletal muscle satellite cells: background and methods for isolation and analysis in a primary culture system. *Methods Mol Biol*. 2012;798:21-52.

Dellavalle A, Sampaolesi M, Tonlorenzi R, et al. Pericytes of human skeletal muscle are myogenic precursors distinct from satellite cells. *Nat Cell Biol*. 2007;9(3):255–267.

DeJong CH, Busquets S, Moses AG, et al. Systemic inflammation correlates with increased expression of skeletal muscle ubiquitin but not uncoupling proteins in cancer cachexia. *Oncol Rep*. 2005; 14(1): 257-263.

Doyle MJ, Zhou S, Tanaka KK, et al. Abcg2 labels multiple cell types in skeletal muscle and participates in muscle regeneration. *J Cell Biol.* 2011;195(1):147–163.

Esfandiari N, Ghosh S, Prado C, et al. Age, obesity, sarcopenia, and proximity to death explain reduced mean muscle attenuation in patients with advanced cancer. *J Frailty Aging.* 2014;3(1):3-8.

Fanin M, Nascimbeni A, Angelini C. Muscle atrophy in Limb Girdle Muscular Dystrophy 2A: a morphometric and molecular study. *Neuropathol Appl Neurobiol.* 2013;39(7):762-771.

Fearon K. Cancer cachexia: developing multimodal therapy for a multidimensional problem. *Eur J Cancer.* 2008;44(8):1124–1132.

Fearon K, Strasser F, Anker SD, et al. Definition and classification of cancer cachexia: an international consensus. *Lancet Oncol.* 2011;12(5):489–495.

Fondazione Centro s, Raffaele del Monte Tabor. Cell Therapy Of Duchenne Muscular Dystrophy by intra-arterial delivery of HLA-identical allogeneic mesoangioblasts. In: Clinicaltrialsregister.eu [Internet]. Italy: Italian Medicines Agency. 2011- [cited 2014]. Available from: <https://www.clinicaltrialsregister.eu/ctr-search/trial/2011-000176-33/IT>
EudraCT Number: 2011-000176-33

Fulle S, Di Donna S, Puglielli C, et al. Age-dependent imbalance of the antioxidative system in human satellite cells. *Exp Gerontol.* 2005;40(3):189–197.

Goodpaster BH, Kelley DE, Thaete FL, et al. Skeletal muscle attenuation determined by computed tomography is associated with skeletal muscle lipid content. *J Appl Physiol.* 2000;89(1):104–110.

Goodpaster BH, Thaete FL, Kelley DE. Thigh adipose tissue distribution is associated with insulin resistance in obesity and in type 2 diabetes mellitus. *Am J Clin Nutr* 2000; 71(4): 885-855592.

Goodpaster BH, Carlson CL, Visser M, et al. Attenuation of skeletal muscle and strength in the elderly: The Health ABC Study. *J Appl Physiol*. 2001;90(6):2157–2165.

Goodpaster BH, Krishnaswami S, Resnick H, et al. Association between regional adipose tissue distribution and both type 2 diabetes and impaired glucose tolerance in elderly men and women. *Diabetes Care*. 2003;26(2):372–379.

Haugaard SB, Mu H, Vaag A, et al. Intramyocellular triglyceride content in man, influence of sex, obesity and glycaemic control. *Eur J Endocrinol*. 2009;161(1):57-64.

He WA, Berardi E, Cardillo VM, et al. NF-kappaB-mediated Pax7 dysregulation in the muscle microenvironment promotes cancer cachexia. *J Clin Invest*. 2013;123(11):4821.

Hicks GE, Simonsick EM, Harris TB, et al. Trunk muscle composition as a predictor of reduced functional capacity in the health, aging and body composition study: The moderating role of back pain. *J Gerontol A-Biol Sci Med Sci* 2005; 60:1420-1424.

Hultman G, Nordin M, Saraste H, et al. Body composition, endurance, strength, cross-sectional area, and density of MM erector spinae in men with and without low back pain. *J Spin Disord* 1993; 6:114-123.

Jang Y, Sinha M, Cerletti M, et al. Skeletal muscle stem cells: effects of aging and metabolism on muscle regenerative function. In: *Cold Spring Harbor Symposia on Quantitative Biology*. Vol 76; 2011:101–111.

Joe AWB, Yi L, Natarajan A, et al. Muscle injury activates resident fibro/adipogenic progenitors that facilitate myogenesis. *Nat Cell Biol.* 2010;12(2):153–163.

Johns N, Stephens N, Fearon K. Muscle wasting in cancer. *Int J Biochem Cell B.* 2013;45(10):2215-2229.

Kalichman L, Hodges P, Li L, et al. Changes in paraspinal muscles and their association with low back pain and spinal degeneration: CT study. *Eur Spine J* 2010; 19:1136-1144.

Kelley DE, McKolanis TM, Hegazi RA, et al. Fatty liver in type 2 diabetes mellitus: Relation to regional adiposity, fatty acids, and insulin resistance. *Am J Physiol Endocrinol Metab* 2003; 285(4): E906-916.

Lanic H, Kraut-Tauzia J, Modzelewski R, et al. Sarcopenia is an Independent Prognostic Factor in Elderly Patients with Diffuse Large B-Cell Lymphoma Treated with Immunochemotherapy. *Leuk Lymphoma.* 2014;55(4):817-823.

Lecker SH, Jagoe RT, Gilbert A, et al. Multiple types of skeletal muscle atrophy involve a common program of changes in gene expression. *FASEB J.* 2004;18:39-51.

Lecourt S, Marolleau J-P, Fromigué O, et al. Characterization of distinct mesenchymal-like cell populations from human skeletal muscle *in situ* and *in vitro* *Exp Cell Res.* 2010;316(15):2513–2526.

Lee S, Kuk JL, Davidson LE, et al. Exercise without weight loss is an effective strategy for obesity reduction in obese individuals with and without type 2 diabetes. *J Appl Physiol* 2005; 99:1220-25.

Lieffers JR, Mourtzakis M, Hall, KD, et al. A viscerally driven cachexia syndrome in patients with advanced colorectal cancer: contributions of organ and tumor mass to whole-body energy demands. *Am J Clin Nutr* 2009; 89: 1173-1179.

Lieffers JR, Baracos VE, Winget M, et al. A comparison of Charlson and Elixhauser comorbidity measures to predict colorectal cancer survival using administrative health data. *Cancer* 2011; 117(9): 1957-1965.

Lindström M, Thornell LE. New multiple labelling method for improved satellite cell identification in human muscle: application to a cohort of power-lifters and sedentary men. *Histochem Cell Biol.* 2009;132(2):141-157.

Lu SH, Wei CF, Yang AH, et al. Isolation and characterization of human muscle-derived cells. *Urology.* 2009;74(2):440-445.

MacDonald AJ, Greig CA, Baracos V. The advantages and limitations of cross-sectional body composition analysis. *Curr Opin Supportive Palliative Care.* 2011;5(4):342–349.

Martin L, Birdsell L, MacDonald N, et al. Cancer Cachexia in the Age of Obesity: Skeletal Muscle Depletion Is a Powerful Prognostic Factor, Independent of Body Mass Index. *J Clin Oncol.* 2013;31(12):1539–1547.

Mackey AL, Andersen LL, Frandsen U, et al. Strength training increases the size of the satellite cell pool in type I and II fibres of chronically painful trapezius muscle in females. *J Physiol.* 2011;589(22):5503–5515.

Mauro A. Satellite cell of skeletal muscle fibres. *J Biophys Biochem Cy.* 1961;9(2):493–495.

McKay BR, Toth KG, Tarnopolsky MA, et al. Satellite cell number and cell cycle kinetics in response to acute myotrauma in humans: immunohistochemistry versus flow cytometry. *J Physiol.* 2010;588(17):3307–3320.

McKay BR, Ogborn DI, Bellamy LM, et al. Myostatin is associated with age-related human muscle stem cell dysfunction. *FASEB J.* 2012;26(6):2509–2521.

Meza-Junco J, Montano-Loza AJ, Baracos VE, et al. Sarcopenia as a Prognostic Index of Nutritional Status in Concurrent Cirrhosis and Hepatocellular Carcinoma. *J Clin Gastroenterol*. 2013;47(10):861-870.

Miljkovic I, Zmuda JM. Epidemiology of myosteator. *Curr Opin Clin Nutr Metab Care*. 2010;13(3):260.

Mitchell KJ, Pannérec A, Cadot B, et al. Identification and characterization of a non-satellite cell muscle resident progenitor during postnatal development. *Nat Cell Biol*. 2010;12(3):257–266.

Mitsiopoulos N, Baumgartner R, Heymsfield S, et al. Cadaver validation of skeletal muscle measurement by magnetic resonance imaging and computerized tomography. *J Appl Physiol*. 1998;85(1):115–122.

Montano-Loza AJ, Meza-Junco J, Baracos VE, et al. Severe muscle depletion predicts postoperative length of stay but is not associated with survival after liver transplantation. *Liver Transplant*. 2014;20(6):640-648.

Montarras D, Morgan J, Collins C, et al. Direct isolation of satellite cells for skeletal muscle regeneration. *Science*. 2005;309(5743):2064-2067.

Mourtzakis M, Prado CM, Lieffers JR, et al. A practical and precise approach to quantification of body composition in cancer patients using computed tomography images acquired during routine care. *Appl Physiol Nutr Metabol*. 2008;33(5):997–1006.

Mozzetta C, Consalvi S, Saccone V, et al. Fibroadipogenic progenitors mediate the ability of HDAC inhibitors to promote regeneration in dystrophic muscles of young, but not old Mdx mice. *EMBO Mol Med*. 2013;5(4):626–639.

Nasis I, Kortianou E, Clini E, et al. Effect of rehabilitative exercise training on peripheral muscle remodelling in patients with COPD: targeting beyond the lungs. *Curr Drug Targets*. 2013;14(2):262-273.

Olguin HC, Olwin BB. Pax-7 up-regulation inhibits myogenesis and cell cycle progression in satellite cells: a potential mechanism for self-renewal. *Dev Biol*. 2004;275(2):375–388.

Pallafacchina G, Blaauw B, Schiaffino S. Role of satellite cells in muscle growth and maintenance of muscle mass. *Nutr Metab Cardiovas*. 2012;23(S1):S12-18.

Pannérec A, Marazzi G, Sassoon D. Stem cells in the hood: the skeletal muscle niche. *Trends Mol Med*. 2012;18(10):599-606.

Pessina P, Conti V, Pacelli F, et al. Skeletal muscle of gastric cancer patients expresses genes involved in muscle regeneration. *Oncol Rep*. 2010;24(3):741-745.

Pietrangelo T, Puglielli C, Mancinelli R, et al. Molecular basis of the myogenic profile of aged human skeletal muscle satellite cells during differentiation. *Exp Gerontol*. 2009;44(8):523–531.

Pisani DF, Dechesne CA, Sacconi S, et al. Isolation of a Highly Myogenic CD34-Negative Subset of Human Skeletal Muscle Cells Free of Adipogenic Potential. *Stem Cells*. 2010;28(4):753-764.

Pisani DF, Clement N, Loubat A, et al. Hierarchization of myogenic and adipogenic progenitors within human skeletal muscle. *Stem Cells*. 2010;28(12):2182–2194.

Poehlman ET, Dvorak RV, DeNino WF, et al. Effects of resistance training and endurance training on insulin sensitivity in nonobese, young women: A controlled randomized trial. *J Clin Endocrin Metab* 2000; 85: 2463-68.

Prado CM, Baracos VE, McCargar LJ, et al. Body composition as an independent determinant of 5-fluorouracil-based chemotherapy toxicity. *Clin Cancer Res*. 2007;13(11):3264–3268.

Prado CM, Lieffers JR, McCargar LJ, et al. Prevalence and clinical implications of sarcopenic obesity in patients with solid tumours of the respiratory and gastrointestinal tracts: a population-based study. *Lancet Oncology*. 2008;9(7):629–635.

Prado CM, Sawyer MB, Ghosh S, et al. Central tenet of cancer cachexia therapy: do patients with advanced cancer have exploitable anabolic potential? *Am J Clin Nutr*. 2013;98(4):1012–1019.

Rasch A, Bystrom AH, Dalen N, et al. Persisting muscle atrophy two years after replacement of the hip. *J Bone Joint Surg Br* 2009; 91:583-588.

Reed SA, Sandesara PB, Senf SM, et al. Inhibition of FoxO transcriptional activity prevents muscle fibre atrophy during cachexia and induces hypertrophy. *FASEB J*. 2012;26(3):987–1000.

Sabel MS, Lee J, Englesbe MJ, Holcombe S. Sarcopenia as a prognostic factor among patients with stage III melanoma. *Ann Surg Oncol*. 2011;18(13):3579–3585.

Sampaolesi M, Blot S, D'antona G, et al. Mesoangioblast stem cells ameliorate muscle function in dystrophic dogs. *Nat*. 2006;444(7119):574–579.

Schiaffino S, Dyar KA, Ciciliot S, et al. Mechanisms regulating skeletal muscle growth and atrophy. *FEBS J*. 2013;280(17):4294-4314.

Schmalbruch H, Hellhammer U. The number of satellite cells in normal human muscle. *Anat Rec*. 1976;185(3):279-287.

Schwarzkopf M, Coletti D, Sassoon D, et al. Muscle cachexia is regulated by a p53-PW1/Peg3-dependent pathway. *Gene Dev.* 2006;20(24):3440–3452.

Shaw JH, Humberstone DA, Douglas RG, et al. Leucine kinetics in patients with benign disease, non-weight-losing cancer, and cancer cachexia: studies at the whole-body and tissue level and the response to nutritional support. *Surgery.* 1991;109(1):37-50.

Shen W, Punyanitya M, Wang Z, et al. Total body skeletal muscle and adipose tissue volumes: Estimation from a single abdominal cross-sectional image. *J Appl Physiol* 2004; 97:2333-2338.

Stephens NA, Gallagher IJ, Rooyackers O, et al. Using transcriptomics to identify and validate novel biomarkers of human skeletal muscle cancer cachexia. *Genome Med.* 2010;2(1):1-12.

Stephens NA, Skipworth RJ, MacDonald AJ, et al. Intramyocellular lipid droplets increase with progression of cachexia in cancer patients. *J Cachexia Sarcopenia Muscle.* 2011;2(2):111-117.

Taaffe DR, Henwood TR, Nalls MA, et al. Alterations in muscle attenuation following detraining and retraining in resistance-trained older adults. *Gerontol* 2009; 55:217-223.

Tan BH, Birdsell LA, Martin L, et al. Sarcopenia in an overweight or obese patient is an adverse prognostic factor in pancreatic cancer. *Clin Cancer Res.* 2009;15(22):6973–6979.

Tandon P, Ney M, Irwin I, et al. Severe muscle depletion in patients on the liver transplant wait list: Its prevalence and independent prognostic value. *Liver Transplant.* 2012;18(10):1209–1216.

Thornell LE. Sarcopenic obesity: satellite cells in the aging muscle. *Curr Opin Clin Nutr.* 2011;14(1):22.

Uezumi A, Fukada S, Yamamoto N, et al. Mesenchymal progenitors distinct from satellite cells contribute to ectopic fat cell formation in skeletal muscle. *Nat Cell Biol.* 2010;12(2):143–152.

Visser M, Kritchevsky SB, Goodpaster BH, et al. Leg muscle mass and composition in relation to lower extremity performance in men and women aged 70 to 79: the health, aging and body composition study. *J Am Geriatr Soc.* 2002;50(5):897–904.

Weber M-A, Krakowski-Roosen H, Schröder L, et al. Morphology, metabolism, microcirculation, and strength of skeletal muscles in cancer-related cachexia. *Acta Oncol.* 2009;48(1):116-124.

Williams A, Sun X, Fischer JE, et al. The expression of genes in the ubiquitin-proteasome pathway is increased in skeletal muscle from patients with cancer. *Surgery.* 1999; 126(4):744-749.

Zampieri S, Doria A, Adami N, et al. Subclinical myopathy in patients affected with newly diagnosed colorectal cancer at clinical onset of disease: evidence from the skeletal muscle biopsies. *Neurolog Res.* 2010;32(1):20-25.